small structures
www.small-structures.com

Vertically Aligned Graphene for Thermal Interface Materials

*Shichen Xu and Jin Zhang**

With the rapidly increasing power density and integration level in electronic devices, the development of the next generation of thermal interface materials (TIMs) with substantially high thermal conductivity is essential for various device technologies. Graphene, exhibiting ultrahigh in-plane thermal conductivity, is investigated intensely for improving the heat dissipation performance. To satisfy the requirements of high vertical thermal conductivity of TIMs, numerous efforts have been made toward the development of the assembly method of graphene sheets extending the intrinsic properties of graphene to macro graphene-based TIMs. A successful approach that erects graphene sheets to construct a vertical structure of graphene material has been widely demonstrated to significantly increase the thermal conductivity of graphene-based TIMs. In this review, the latest advances in the rational design and controllable fabrication of vertical graphene structures by means of top-down and bottom-up methods are summarized. Moreover, the state-of-the-art progress on graphene-based TIMs is discussed from the viewpoint of material fabrication, structure design, and property optimization. Finally, the existing advantages, challenges, and perspectives of high-thermal-conductivity graphene-based TIMs are presented and highlighted.

1. Introduction

Along with the technology evolution toward miniaturization, dense integration, and high power in electronic devices, the heat flux density generated in a unit area increases rapidly, which will seriously shorten the service life of electronic devices. Therefore, exploring efficient heat dissipation technologies has gradually become key for the development of electronic components.[1–4] Thermal interface materials (TIMs), which function in enhancing heat transport at rough and uneven mating surfaces, play a very important role in solving the interfacial heat transfer problem.[5–7] In particular, TIMs yielding high vertical thermal conductivity can transfer heat effectively. However, the vertical thermal conductivity of commercial TIMs is normally limited to $10\,W\,m^{-1}\,K^{-1}$(usually around 4 or $5\,W\,m^{-1}\,K^{-1}$), which is far from satisfying the requirement in efficient thermal management of power devices.[8] Therefore, how to dramatically improve the thermal conductivity of TIMs is still an imperative challenge.

Graphene, regarded as the most promising candidate for thermal management in both academics and industry, has been widely used in heat dissipation in-plane or out-of-plane due to its extremely high thermal conductivity and excellent mechanical strength.[9,10] Traditional TIMs are mainly formed with graphene composites composed of graphene powder and polymer complex by solution methods.[11] Due to the high thermal contact resistance derived from the weak coupling between the graphene skeleton and the polymer matrix, the random arrangement of graphene sheets and the presence of polymer resins seriously reduce the vertical thermal conductivity of the graphene-composite-based TIMs. To construct TIMs with excellent thermal conductivity, graphene sheets with high in-plane thermal conductivity need to be erected and assembled orderly in the vertical direction so that the intrinsic thermal properties of graphene can be fully extended and utilized in TIMs.

However, the arrangement and assembly strategies of graphene sheets play a decisive role in transmitting the thermal properties of the graphene microstructure to the macroscopic graphene materials. Here, aiming at the applications in high-performance TIMs toward heat dissipation systems, we focus on the progress in the special design and controllable preparation of graphene materials with desired architectures. As shown in **Figure 1**, to produce high-performance TIMs, graphene sheets need to be vertically aligned and assembled. The preparation strategies of vertical graphene (VG) structures with high thermal conductivity can be summarized as top-down and bottom-up methods. The top-down methods are mainly represented by mechanical processing and hydrothermal reduction with graphene oxide (GO) or reduced graphene oxide (rGO) as raw materials.[13–16] On the contrary, the bottom-up methods are mainly represented by plasma enhanced chemical vapor deposition (PECVD), by which VG with a specific morphology can be directly grown using different types of carbon sources as precursors.[12,17] This review attempts to summarize the state-of-the-art research on the preparation of VG to provide guidelines on the design of VG structures and discusses the progress and

S. Xu, Prof. J. Zhang
Center for Nanochemistry
Beijing Science and Engineering Center for Nanocarbons
Beijing National Laboratory for Molecular Sciences
College of Chemistry and Molecular Engineering
Peking University
Beijing 100871, P. R. China
E-mail: jinzhang@pku.edu.cn

S. Xu, Prof. J. Zhang
Division of Graphene Fiber Technology
Beijing Graphene Institute
Beijing 100095, P. R. China

The ORCID identification number(s) for the author(s) of this article can be found under https://doi.org/10.1002/sstr.202000034.

DOI: 10.1002/sstr.202000034

 © 2020 Wiley-VCH GmbH

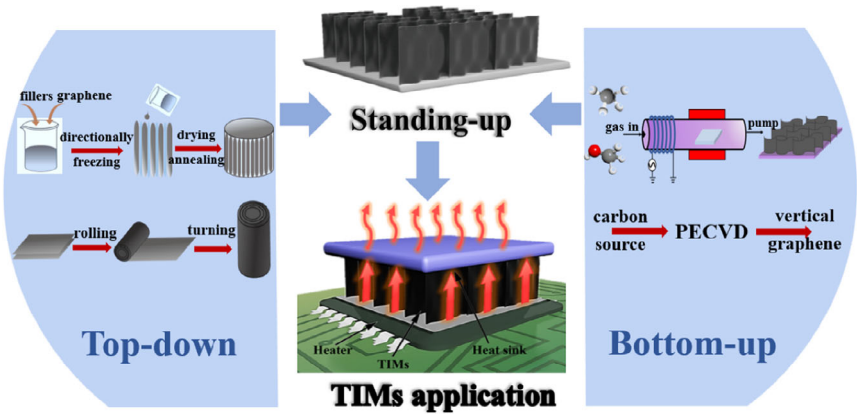

Figure 1. Schematic diagram of VG for TIMs. The middle section shows that upright graphene is beneficial for TIMs. The left and right sections show the top-down and bottom-up approaches to preparing VG, respectively. The schematic illustration of TIMs is reproduced with permission.[12] Copyright 2020, Wiley-VCH.

advantages of VG-based TIM applications to offer a perspective on the preparation of VG for TIM applications.

2. Preparation of VG Structure

In this part, we mainly discuss the preparation methods of VG structures consisting of VG arrays,[12] VG monoliths,[16] VG aerogels,[18] etc. The preparation methods are divided into top-down methods and bottom-up methods according to the different approaches to assembling raw materials. One of synthesizing VG by self-assembly of GO sheets[16,18–25] or organic supermolecules with benzene rings[26] belongs to the top-down method, while the others of synthesizing VG by splicing together carbon fragments or carbon atoms are classified as the bottom-up methods. In the following sections, we will discuss these two different methods for preparing VG in detail.

2.1. Top-down Method

The top-down methods are used to form the VG structure by assembly of some molecules with benzene rings or GO sheets, including molecular self-assembly,[26] rolling–cutting,[19–21,23] directionally freezing,[22,25] oriented hydrothermal reduction, and the shrinking–compressing method.[16] The common characteristics of these methods are that the preparation processes are based on solution phase and are dependent on high-temperature annealing. High temperature is beneficial to carbonization of organic supermolecules or reduction and graphitization of GO sheets.

2.1.1. Molecular Self-Assembly Method

As shown in **Figure 2**a, Hurt and coworkers used chromonic liquid crystal (CLC) precursors to fabricate vertically aligned graphene layer arrays on substrates.[26] Oriented liquid crystal phases were spontaneously formed in aqueous solution when organic dyes reached a high concentration. Parallel orientation of the supramolecular rods composed of water-soluble organic dyes on substrates produced a set of vertically aligned disks in the presence of shear or elongational flow. Then, the orientation of the disk-like molecules on substrates became stabilized through edge-to-edge polymerization reactions during room-temperature drying and a high-temperature carbonization process, in which neighboring molecular disks cross-link and merge into VG layers with retention of the vertical order.

2.1.2. Rolling–Cutting Method

A typical schematic diagram of the preparation of VG by the rolling–cutting method is shown in Figure 2b. Ethanol was sprayed onto dried GO paper to facilitate good adhesion between graphene films in the rolling process. Then, the rolled GO paper was cut into pieces across the cross-section. Meanwhile, the cut-rolled strips of the horizontally rolled GO paper were erected to be a vertically oriented GO films. Eventually, vertical rGO films were obtained after a high-temperature reduction. By this method, Lee and coworkers fabricated highly dense and vertically aligned rGO for capacitor applications.[19] In addition, by adding polymer resin to the coiled graphene, Bai and coworkers prepared thermally reduced vertically aligned rGO film/epoxy composites.[20,21,23]

2.1.3. Directional-Freezing Method

Schematic illustration of the fabrication of vertically aligned graphene aerogels using directional freezing is displayed in Figure 2c. Yu et al. synthesized vertically aligned, ultralight, and highly compressive all-graphitized graphene aerogels by chemical reduction of GO suspension followed by directional freezing and freeze drying.[25] Wong and coworkers prepared vertically aligned and interconnected graphene networks based on a controllable three-step strategy, including formation of GO liquid crystals, oriented freeze casting, and annealing reduction under an argon atmosphere.[22] In this approach, the directional growth of GO liquid crystals along the ice template resulted in the formation of a VG structure, and the sublimation of the ice crystal ultimately led to the formation of an aligned and porous graphene material.

 © 2020 Wiley-VCH GmbH

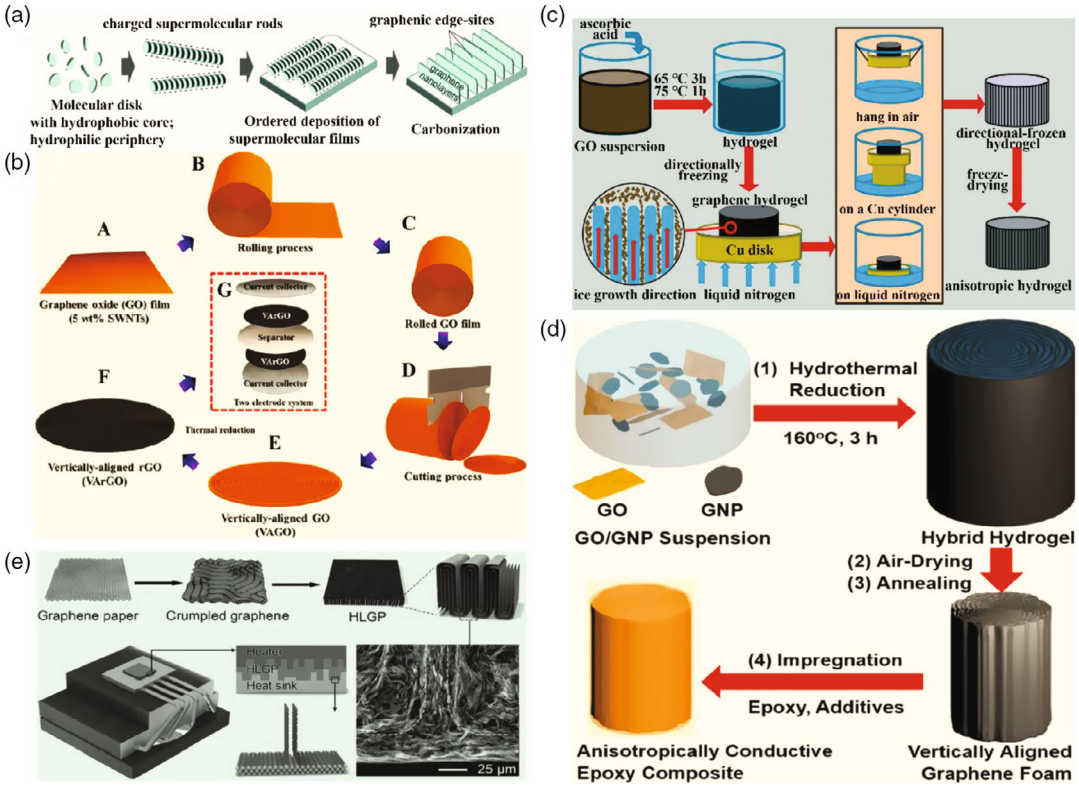

Figure 2. The top-down method for preparation of VG structure. a) Molecular self-assembly method. Reproduced with permission.[26] Copyright 2011, Wiley-VCH. b) Rolling–cutting method. Reproduced with permission.[19] Copyright 2014, American Chemical Society. c) Directional-freezing method. Reproduced with permission.[25] Copyright 2018, Elsevier. d) Oriented hydrothermal reduction method. Reproduced with permission.[24] Copyright 2018, American Chemical Society. e) Shrinking–compressing method. Reproduced with permission.[16] Copyright 2019, American Chemical Society.

2.1.4. Oriented Hydrothermal Reduction Method

Vertically aligned high-quality graphene foams were synthesized by hydrothermally assembling a suspension of GO sheets followed by drying and annealing. As shown in Figure 2d, the preparation of vertically aligned foams was mainly through three processes: hydrothermal reduction, air drying, and vacuum annealing. By adding boron nitride nanosheets (BNs)[18] and graphite nanoplates (GNPs)[24] to the hydrothermal system, Yu et al. fabricated rGO/BN and rGO/GNP hybrid aerogels with a long-range ordered architecture, respectively. During the self-assembly of GO sheets by π–π interactions, BN and GNP were wrapped and connected by GO sheets due to van der Walls interactions, resulting in a similar vertically aligned hybrid network.

2.1.5. Shrinking–Compressing Method

The machining process is a purely physical top-down approach. In addition to cutting the rolled graphene paper, formation of a vertically aligned architecture could also be realized when applying a lateral mechanical force to stacked graphene paper. As shown in Figure 2e, Lin and coworkers adopted a simple machining method to modulate the alignment of graphene microstructure.[16] A VG monolith was synthesized by a two-step mechanical machining process. A specific lateral force was first applied around the stacked graphene paper, generating the formation of crumpled graphene. The lateral compression of this crumpled structure would contribute to a compact vertical monolith.

2.1.6. Self-Aligning "Magnetic Graphene" Filler Method

Balandin and coworkers developed a unique method for the preparation of self-aligning "magnetic graphene" fillers.[27] In this method, polymer wrapping technique and layer-by-layer self-assembly strategies were used to achieve the noncovalent attachment of nanoparticles to the surface of graphene and few-layer graphene (FLG), which were obtained by the scalable liquid-phase exfoliation method. Poly-sodium-4- styrene sulfonate was used to wrap graphene and polyelectrolyte poly-dimethyl-diallylammonium chloride was used to produce homogeneous positive charges, which adsorbed negatively charged magnetic nanoparticles onto the surface of graphene and FLG under the electrostatic interactions. Finally, the functionalization of graphene flakes with magnetic nanoparticles was beneficial for the alignment of graphene fillers in an external magnetic field during dispersion of the thermal paste to the connecting surfaces.

In summary, in addition to self-assembly of organic supermolecules, the top-down methods were mainly used to prepare VG

 © 2020 Wiley-VCH GmbH

by self-assembly of GO sheets in solution phase. GO can be produced by many different strategies, most typically by the modified Hummer's method. This method was exceptionally feasible in creating a scalable production of GO exhibiting great potential and significant advantages in the rapid batch preparation of large quantities of macroscopic VG materials. In short, the top-down method is promising for mass production of VG.

2.2. Bottom-up Method

PECVD is a typical bottom-up method for directly preparing VG. In the PECVD system, carbon sources are activated, dissociated, and ionized by the high-energy electrons generated in the plasma system, and further the excited carbon species results in the growth of VG on various substrates.[28–31] PECVD exhibites several advantageous features, such as a relatively low growth temperature, high growth selectivity, and free metal catalysts. However, the complexity of plasma chemistry makes the growth mechanism of VG elusive. In addition, the growth of VG in PECVD is affected by many factors. Especially, the morphology and structure of the VG sheets produced by PECVD are strongly dependent on the types of plasma sources and a series of operating parameters, such as feedstock gas type and composition, substrate temperature, and operating pressure. It is crucial to understand the influence of different factors on the growth rate and morphology of VG. Therefore, in this section, we first discuss the growth mechanism of VG in PECVD, and then summarize the factors affecting the growth of VG, especially focusing on the growth rate and morphology of VG.

2.2.1. Growth Mechanism of VG in PECVD

Although it still remains elusive and puzzling in explaining the growth process in PECVD, a critical three-step nucleation and growth mechanism of VG was generally accepted. These three steps can be described briefly as follows.

Formation of Nucleation Sites: There were even controversial explanations for VG nucleation. As shown in **Figure 3**a, some evidence was presented for the formation of a buffer layer on the substrate, which served as nucleation sites for the VG growth. The buffer layer formed in the nucleation step is usually made of either amorphous carbon or carbide.[32] Amorphous carbon is formed due to the large mismatch of the lattice parameters between the substrate material and the graphite, while a carbide layer is formed when the substrate reacts with carbon atoms.[35–37] In addition, VG adjoined to carbon onions is also observed in Figure 3b. Similar to the buffer layer, the carbon onions also serves as active nucleation sites for the growth of VG.[32] Once the buffer layer or carbon onion–like graphitic layer is formed, the graphene nanosheets starts to grow.

Growth of VG Sheets: VG with open edges originates from the mismatches and curved areas of the graphitic layer and continuously grows vertically under the influence of internal stress and a localized electric field. Internal stress is accumulated between the graphitic layer and substrate arising from the temperature gradients, ion bombardment, and lattice mismatch between the substrate and graphitic layer, which results in upward growing of aligned graphene sheets. The local electric field is induced in the plasma sheath, which can effectively control the orientation, density, and spatial distribution of the VG. As shown in Figure 3c (left), a continuum model based on the surface diffusion was proposed to describe the continuous growth of graphene.[32] Carbon atoms landed on the surface of graphene sheets, subsequently diffused along the sheets, and continuously incorporated into the open edges for continuous growth of VG. In addition, this model also indicates that VG growth only occurred at open edges, as shown in Figure 3c (right) and Figure 3d, which indicates that the presence of seamless or folded edges would terminate the growth.[33]

Growth Termination: The growth of VG finally terminates upon the closure of open edges determined by the competition between carbon deposition and etching effects in the plasmas. The presence of amorphous carbon at the edge or on the sheets' surface would accelerate the tendency of active edge closure and increase the possibility of growing multilayer graphene. The etching growth mechanism was beneficial to slowing down edge closure and promoting VG growth.[12,34,38] As shown in Figure 3e,f, the hydrogen atoms decomposed from alkanes or the hydroxyl groups decomposed from the alcohol could act as etchants to rapidly remove amorphous carbon for preventing the formation of secondary nucleation and removing cross-linking at the active edges, thus, promoting a continuous growth of highly crystalline graphene.

The generally accepted three-step growth mechanism helps us to better understand the growth process. However, exploring the growth mechanism is fundamental to the controllable growth of VGs, and the subsequent accurate analysis and regulation of the factors affecting growth are key to preparing high-quality VG.

2.2.2. Factors Affecting Growth of VG in PECVD

The morphology and structure of VG sheets grown with PECVD are strongly affected by a series of operating parameters, including feedstock gas type, gas proportion, system temperature, operating pressure, operating power, and plasma type. In this section, we discuss these important operating parameters for the synthesis of VG in the PECVD process, especially the plasma types.

In **Figure 4**, PECVD is classified into six categories according to the types of plasma sources, including microwave PECVD (MW-PECVD), direct current PECVD (DC-PECVD), inductively coupled PECVD (IC-PECVD), capacitively coupled PECVD (CC-PECVD), alcohol-based electric-field-assisted PECVD (AEF-PECVD), and hybrid PECVD (H-PECVD). **Figure 5**a–c schematically illustrates MW-PECVD, which yields high-frequency electromagnetic radiation in the gigahertz range.[39–41] Because the electric field and magnetic field are perpendicular to the direction of wave travel, MW-PECVD can be divided into transverse magnetic (TM) mode MW-PECVD[39] and transverse electric (TE) mode MW-PECVD,[40] which are shown in Figure 5a,b, respectively. DC-PECVD is characterized by the application of a sufficient potential between the cathode and the anode. As schematically shown in Figure 5d,e, pin-to-plate electrode pair[42] and parallel-plate electrode pair[17] are the two main setups of DC-PECVD used to synthesize VG. Radio frequency (RF) PECVD mainly includes IC-PECVD (ICP) and CC-PECVD (CCP). According to the plasma generated by the planar coil

© 2020 Wiley-VCH GmbH

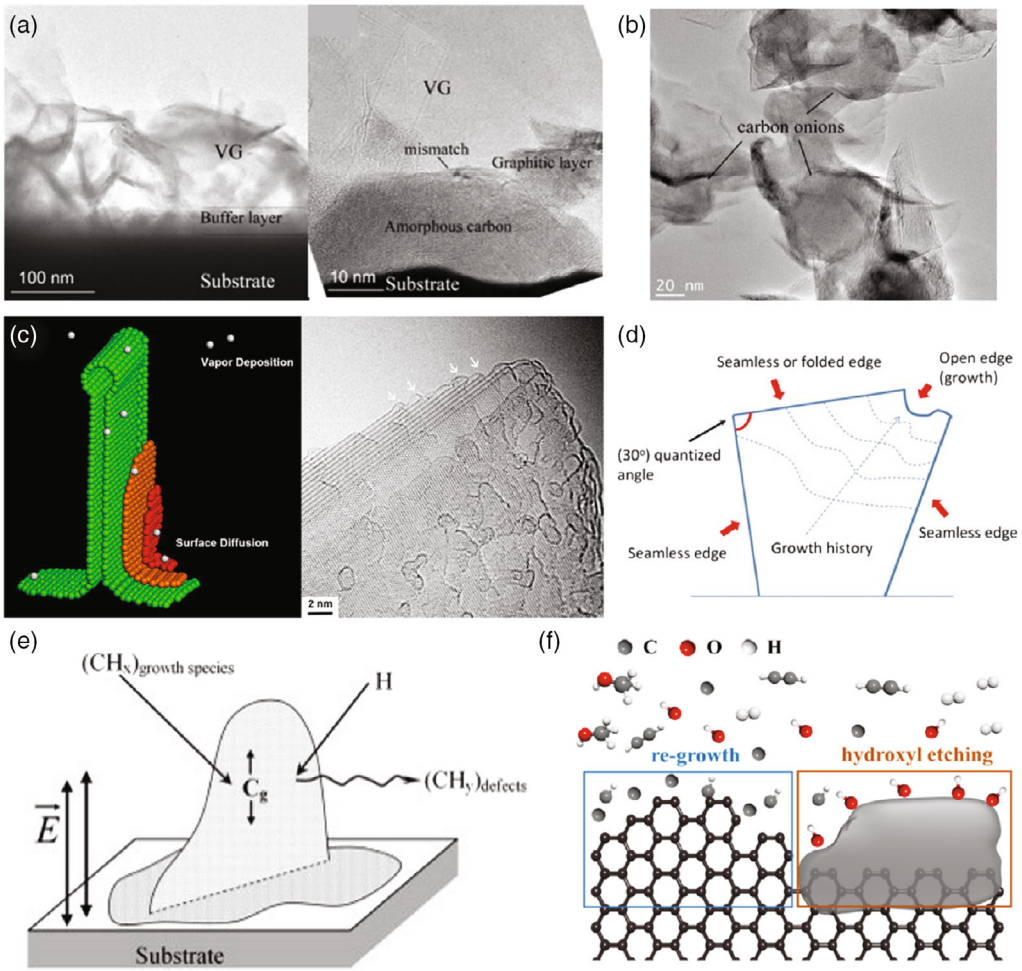

Figure 3. Growth mechanism of VG. a,b) Formation of nucleation sites: buffer layer or carbon onion–like graphitic layer. c) A continuum model based on the surface diffusion. (a–c) Reproduced with permission.[32] Copyright 2014, American Chemical Society. d) Schematic representation of VG with folded/seamless and open edges. Reproduced with permission.[33] Copyright 2014, Elsevier. e) A schematic of VG growth controlled by carbon surface diffusion. Reproduced with permission.[34] Copyright 2007, Elsevier. f) Etching effect for regrowth of VG. Reproduced with permission.[12] Copyright 2020, Wiley-VCH.

or helicon antenna, IC-PECVD is also divided into evanescent electromagnetic (H) mode[43] and propagating wave (W) mode.[44] H-mode and W-mode IC-PECVD are shown in Figure 5f,g, respectively. Figure 5h is a schematic diagram of CC-PECVD.[45] Despite CC-PECVD using a simpler apparatus, the relatively low electron density makes CC-PECVD rarely be used to grow VG individually. Moreover, as is the same with CC-PECVD, DC-PECVD is also used for growing VG in combination with other high-density plasma sources making up H-PECVD, such as CCP + ICP,[46] CCP + MW,[47] and DC + MW,[48] as shown in Figure 5i,j,k, respectively.

PECVD has diverse types of plasma sources and different configurations, which also contribute to the complexity of the plasma chemistry. The microwave plasma source has high energy, which promotes the rapid growth of VG, while the generator of CC-PECVD is equipped with parallel electrode plates, which is conducive to the vertical directional growth of VG. The morphology and structure of the VG sheets produced by PECVD are strongly dependent on the types of plasma sources. The growth of VG by PECVD is an extremely complex process, which is influenced by many factors simultaneously. Only by precisely regulating the growth conditions of VG can the controllable preparation of high-quality VG be realized.

As shown in Figure 4, apart from plasma type, there are some other factors affecting VG growth.[49–51] 1) Feedstock gas type: Different carbon sources with diverse dissociation energy result in different growth rate and morphology of graphene. 2) System temperature: The substrate temperature has a great influence on the PECVD process because it strongly affects the reaction kinetics. 3) Operating pressure: The system pressure can regulate the ionization rate and maintain the stability of the plasma. 4) Gas proportion: The composition and proportion of the feedstock gas significantly affect plasma properties and type of active species, as well as the morphology and quality of the VG. 5) Operating power: The power of the plasma determines the dissociation rate of the carbon source and the concentration of the active species.

 © 2020 Wiley-VCH GmbH

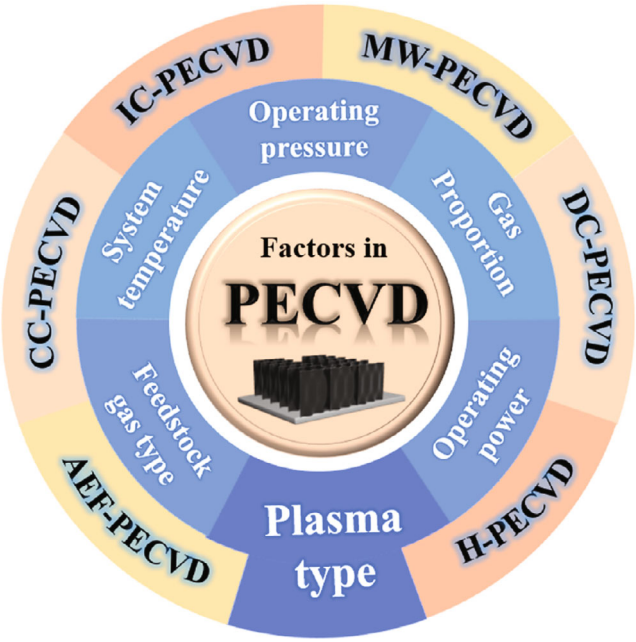

Figure 4. Factors influencing the growth of VG in PECVD.

These factors mainly affect the morphology and growth rate of VG. More details and examples will be discussed in Section 2.2.3.

2.2.3. Morphology and Growth Rate of VG in PECVD

The controllable growth of VG has always been a key concern. Some important reviews have summarized the growth and applications of VG prepared by PECVD.[49–51] To extensively explore more applications, it is essential to achieve rapid growth of VG. In this section, we focus on the morphology and growth rate of VG in PECVD.

Table 1 lists some typical experimental conditions and corresponding growth results[31,35–38,41,46,47,52,54–63,65–69] indicating that diverse morphologies of graphene in different plasma systems were grown with various growth velocities. The diverse morphologies of VG can be simply classified into "random" type and "vertical" type, which are related to the plasma types, plasma power, and carbon sources. The typical morphology of the so-called random type of VG appears petal-like[59] and forest-like,[68] while the height and thickness of the so-called vertical type of VG are always uneven and various.[37,60,66]

There are two important factors affecting VG alignment, i.e., plasma type and vertical force. When the energy of the plasma is not high enough to decompose the carbon source sufficiently, it is easy to generate amorphous carbon to prevent the graphene from growing vertically. In addition, when the vertical force is insufficient for carbon atoms to migrate and diffuse on the graphene sheets, the vertical growth of the graphene sheets will also be inhibited. As shown in Table 1, CCP alone as a plasma for VG growth is commonly insufficient due to the relatively low electron density and electron energy. As an alternative, CCP together with other high-density plasma, such as CCP + ICP, benefits both the growth rate and the alignment of VG sheets during growth.[46] Similarly, when using MW plasma or DC plasma separately, it is difficult to achieve fully vertical growth of graphene, while graphene can be grown perpendicular to the substrate using coupled MW and DC plasma.[55–57] The MW plasma yields a strong energy for decomposition of the carbon source, and simultaneously the DC plasma generator induces a vertical electric field when a voltage is applied. Therefore, the hybrid MW + DC plasma can naturally promote the rapid growth of oriented VG. However, in addition to generating the electric field by the plasma generator itself, establishing an electric field in the reaction system artificially could also create the force in the growth direction of VG.[70,71] Zhang and coworkers introduced a built-in electric field in a PECVD system for the alignment of the graphene sheets.[12] Their results proved that 3D staggered graphene nanowalls were synthesized when no electric field was exerted, while VG arrays perpendicular to the substrates were grown when applying an in-built vertical electric field. This study convincingly demonstrated the important role of the electric field for alignment of VG.

Compared to the factors affecting the morphology of VG, there are more factors influencing the growth rate of VG, including the type of plasma, the power of the plasma generator, the temperature and pressure of the system, the type of carbon source, the strength of the electric field force, and the catalyst.

The type of plasma determines the density of high-energy electrons, which are used for excitation and ionization of carbon sources. The typical electron density of CCP (10^9–10^{10} cm^{-3}) is obviously lower than those of MW and ICP plasmas (10^{10}–10^{13} cm^{-3}), which is the main reason why VG grown in MW-PECVD and IC-PECVD has a higher growth rate.[49] The operating power of PECVD directly influences the concentration and energy of the plasma, which is used to produce high-energy electrons and active species. The higher the power of the plasma generator, the higher the energetic electrons and higher the concentrations of the carbon active species that can be produced, which will eventually accelerate the growth of VG.[68] Furthermore, VG growth in a PECVD process usually can be operated at a temperature of several hundred degrees. In addition to assisting in the decomposition of carbon sources, the heat energy is more beneficial to heat the substrate.[64,72] The substrate temperature is of great importance for the PECVD process as it strongly affects the surface reaction kinetics. Therefore, a relatively high temperature determines faster growth of VG. Another important parameter that significantly influences the plasma properties and growth rate is the operating pressure, which is inversely proportional to the mean free path of electrons.[49,72,73] A high pressure means a short mean free path of electrons and subsequent inhibition of the ionization of carbon sources. However, a higher reaction pressure accommodates a larger volume of feedstock gas, which could realize the growth of vertically oriented graphene at a relatively high growth rate.

The selection of the carbon source is critical, especially for the growth rate of VG. Hydrocarbon (C_2H_2 or CH_4) is the most popular choice of carbon source for PECVD systems, in which C_2 dimers play a key role in the growth rate.[74] Compared with CH_4, which produces C_2 through radical dissociation and subsequent recombination, C_2H_2 is able to produce C_2 through direct dissociation due to the strong C≡C bond. Zhu et al. compared

© 2020 Wiley-VCH GmbH

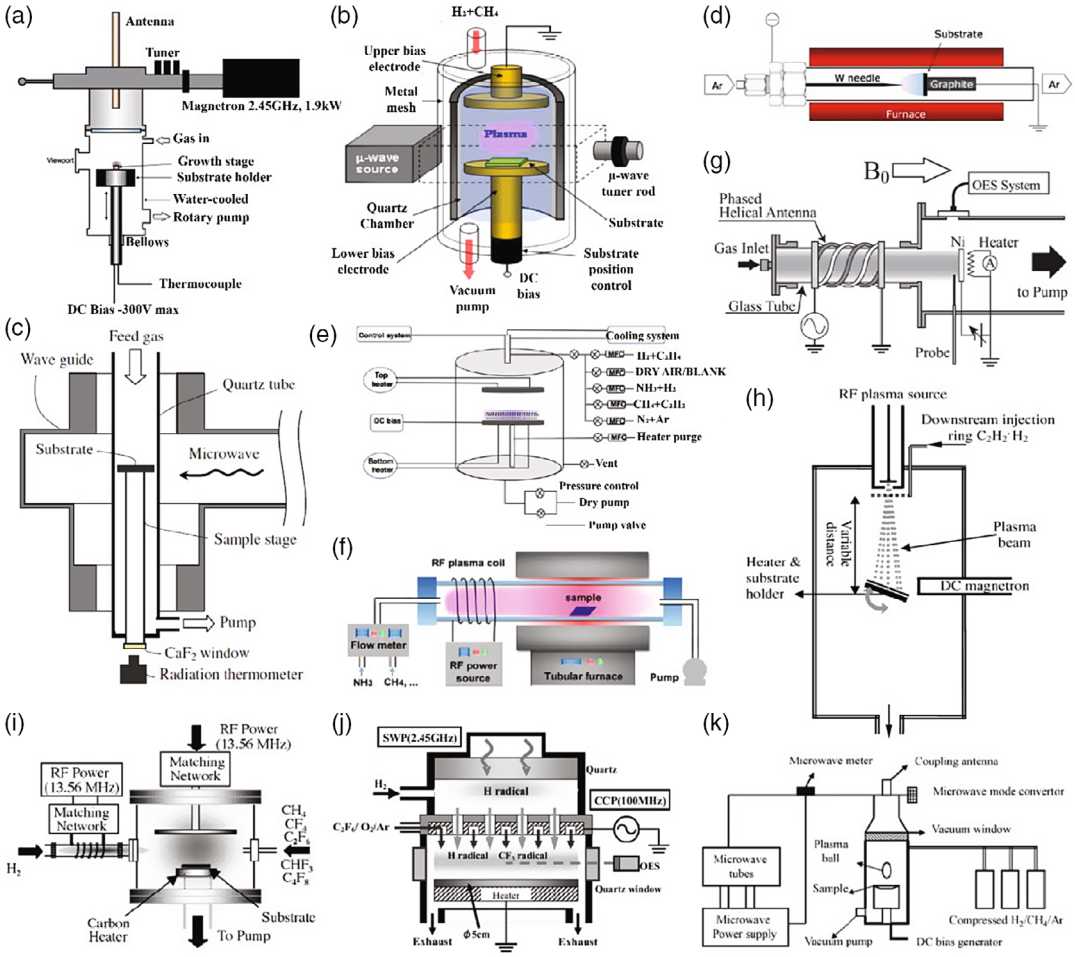

Figure 5. Schematic diagrams of various PECVD systems for VG growth. a) TM mode MW-PECVD. Reproduced with permission.[39] Copyright 2006, Elsevier. b) TE mode MW-PECVD. Reproduced with permission.[40] Copyright 2010, American Institute of Physics. c) MW-PECVD. Reproduced with permission.[41] Copyright 2011, Elsevier. d) Pin-plate DC-PECVD. Reproduced with permission.[42] Copyright 2011, Springer. e) Parallel-plate DC-PECVD. Reproduced with permission.[17] Copyright 2019, Wiley-VCH. f) Coil-equipped IC-PECVD. Reproduced with permission.[43] Copyright 2015, American Chemical Society. g) Helicon IC-PECVD. Reproduced with permission.[44] Copyright 2006, Japan Society of Applied Physics. h) Expanding CC-PECVD. Reproduced with permission.[45] Copyright 2010, Institute of Physics Publishing. i) ICP + CCP. Reproduced with permission.[46] Copyright 2005, Elsevier. j) CCP + MW. Reproduced with permission.[47] Copyright 2008, American Institute of Physics. k) DC + MW. Reproduced with permission.[48] Copyright 2008, Elsevier.

the growth of VG in IC-PECVD using CH_4 and C_2H_2 precursors.[65] They found that VG grown with C_2H_2 had a smoother surface, more uniform distribution, better ordered vertical orientation, and about eight times higher growth rate, in comparison with VG prepared with CH_4. In addition, fluorocarbons (CF_4, CHF_3, and C_2F_6) have also been used to prepare VG. Hori and coworkers conducted a comparative work on VG synthesis using a series of fluorocarbons; then they found that the growth rate decreased in the order of $C_2F_6 > CHF_3 > CF_4$.[46] CF_3 radicals are important species responsible for the formation of VG, and the concentration of CF_3 radicals determines the growth rate of VG. C_2F_6 was expected to yield CF_3 radicals most effectively; therefore, C_2F_6 yielded a relatively more rapid growth of VG. In addition to the active carbon species decomposed from carbon sources, species that can etch amorphous carbon also have an effect on the growth rate. Zhang and coworkers compared as-grown VG using CH_4 and CH_3OH, then they concluded that OH radicals have a stronger ability to etch amorphous carbon to promote rapid growth of VG.[12]

As an indispensable force for the growth of VG, the electric field force can not only control the direction of the graphene sheets mentioned previously,[12,70,71,75] but also accelerate the diffusion and migration of carbocations on the graphene sheet, thus promoting the rapid growth of VG. Ostrikov and coworkers achieved the transformation from a horizontal graphene layer to a directed individual graphene sheet by reorienting the direction of the built-in plasma electric field.[71] They found that when the angle between the electric field and the substrate was 90°, the as-grown VG was the highest, indicating that the vertical electric field forces accelerated the growth of graphene. Zhang and coworkers used electric-field-assisted PECVD to significantly accelerate the growth rate of VG by introducing a

 © 2020 Wiley-VCH GmbH

Table 1. Overview of PECVD processes for VG synthesis.

Plasma source	Power/voltage	Precursor	Growth time [h]	Height [μm]	Growth rate [μm h^{-1}]	Vertical/random
DC[52]	50–250 V	CH_4	–	0.5–3	–	Vertical
DC[31]	250 V	CH_4	0.75	4	5.33	Random
DC[53]	750–800 V	CH_4	1	–	–	Random
DC[54]	150 W	CH_4	0.25	0.09	0.36	Random
DC + MW[55]	200 V + 500 W	CH_4	1	38	38	Vertical
DC + MW[56]	185 V + 500 W	CH_4	0.25	2.5	10	Vertical
DC + MW[57]	200 V + 500 W	CH_4	0.33	–	–	Vertical
MW[58]	1500 W	CH_4	0.5	–	96	Random
MW[59]	2000 W	CH_4	0.83	–	–	Random
MW[60]	800 W	CH_4/C_2H_2	0.5	30	60	Vertical
MW[41]	60 W	CO	0.025	1.5	60	Both
MW[39]	500 W	C_2H_2	0.17	–	–	Random
MW + CCP[61]	270 W + 250 W	C_2F_6	–	0.72	–	Random
MW + CCP[47]	250 W + 300 W	C_2F_6	0.5–2	–	–	Vertical
CCP[62]	400 W	C_2H_2	–	12	–	Vertical
CCP + ICP[63]	100 W + 400 W	C_2F_6	8	<1.6	<0.2	Vertical
CCP + ICP[46]	100 W + 400 W	$CH_4\backslash CF_x$	8	<1.6	<0.2	Vertical
ICP[64]	900 W	CH_4	–	–	<4.5	Random
ICP[65]	1000 W	C_2H_2	0.17	2.72	16	Vertical
ICP[35]	1000 W	CH_4	0.67	3.1	4.5	Both
ICP[66]	300 W	CH_4	1	0.13	0.13	Random
ICP[37]	500 W	CH_4	0.5	1.5	3	Vertical
ICP[67]	280 W	C_2H_2	0.2	0.27	1.35	Vertical
ICP[68]	280 W	C_2H_2	2	7	3.5	Random
ICP[38]	300 W	C_2H_5OH	0.5	0.07	0.14	Random

built-in electric field into the reaction system.[12] Moreover, they also found that the growth rate of VG increased with the electric field intensity.

Surprisingly, the catalyst also promoted the growth of VG. Catalysts are widely used in the growth of carbon materials because they can reduce the dissociation energy barrier of the carbon source. PECVD is well known as a catalyst-independent process. However, when a catalyst is introduced into the system, it also accelerates VG growth.[76] Chae and coworkers directly prepared VG on glass substrates by a one-step copper-assisted PECVD process.[67] The growth rate of the VG was enhanced by a factor of 5.6 when a piece of copper foil was located around a glass substrate as a catalyst in the system.

Although the morphology and growth rate of VG are affected by many factors, it does not hinder the wide application of VG in many fields such as electrocatalysis and energy because of its excellent and unique properties. These properties are closely related to the vertical structure of graphene sheets. Obviously, controlling the preparation of VG is critical to expanding the applications of VG. Therefore, only by continuously optimizing the growth conditions and regulating the growth factors can VG be prepared with application value.

3. VG in TIM Applications

VG structures have some unique morphological and structural features, such as vertical orientation and high specific surface area, which make them significantly different in many aspects from the conventional horizontally or randomly oriented graphene. Combined with the intrinsic overwhelming electrical, chemical, and mechanical properties of graphene, VG shows great potential in emerging applications ranging from energy and environmental applications to electrocatalytic applications.[50,51,57,77–81] For examples, the large specific surface area and high electrical conductivity can promote VG use in electrochemical capacitors and solar cells;[50,51,58,77–82] the high density of open edges can enhance the chemical and electrochemical activity in sensors;[58,82] and the high aspect ratio and electrical conductivity can facilitate generation of atmospheric corona discharges.[83,84] It is worth noting that in addition to the unique electrical, mechanical, and chemical properties of graphene, its excellent thermal properties make it widely used for heat dissipation.[8,85–87] To satisfy the requirements of high vertical thermal conductivity of TIMs, a successful approach that erects graphene sheets for construction of a vertical-structured graphene-based TIM has been widely demonstrated to increase the thermal conductivity in the vertical direction.

© 2020 Wiley-VCH GmbH

3.1. Metal and Ceramic for TIMs

In fact, before graphene-based materials were used as TIMs, metal and ceramic materials had been explored to build TIMs.[88] The metal acted as a TIM in the form of a solder or thermal conduction additive. Solders can provide a continuous metal phase for heat transfer. Alloy solders were investigated as TIMs, in which the metals partly diffused into each other, leading to the formation of intermetallic compounds. Li and coworkers investigated the contact thermal resistance of a Sn–Bi solder paste between two Cu plates and demonstrated the feasibility of the Sn–Bi solder paste in TIM applications.[89–92] Its thermal interface resistance was less than 10 K mm^2 W after thermal cycling, indicating that the Sn–Bi solder paste with high thermal conductivity could be a promising candidate for TIM application in power electronics devices. Similar to metal particles, ceramics with high thermal conductivity were used as additives in polymer resins or metal solders to construct TIMs. Guo and coworkers synthesized an epoxy matrix composite adhesive containing aluminum nitride (AlN) ceramic powder.[93] This epoxy-ceramic based TIM obtained excellent thermal conductivity, which was ≈13 times larger than that of pure epoxy. Mustafa et al. developed a new TIM that covalently connected functionalized BN and a copper-solder matrix by soft organic ligands.[94] The metal–inorganic–organic hybrid nanocomposite demonstrated high bulk thermal conductivities ranging from 211 to 277 W m^{-1} K^{-1}.

3.2. Different Structure of Graphene Materials for TIMs

It is well known that metals and ceramics have high thermal conductivity and therefore can be used as suitable candidate materials for construction of TIMs. However, with electronic devices moving toward miniaturization and light weight, graphene with ultrahigh thermal conductivity exceeding 5000 W m^{-1} K^{-1} is attracting a lot of attention and seems to be the best building material for the development of new flexible, lightweight TIMs. Recently, numerous graphene-based TIMs have been explored, including planarly oriented graphene paper, randomly arranged graphene composites, and vertically aligned graphene materials. Graphene-based TIMs with different structures exhibit different thermal conductivity; especially TIMs composed of vertical graphene structures exhibit the best thermal conductivity.

3.2.1. Planarly Oriented Graphene Film for TIMs

Flexible graphene paper/film assembled from graphene sheets has been fabricated by solution-based methods, such as direct evaporation,[95] vacuum filtration,[53] direct electro-spray deposition,[96] and scanning centrifugal casting.[97] Planar graphene paper has been commonly used as an in-plane thermal spreading material, due to its excellent in-plane thermal conductivity.[98,99] Recently, some research effort has been devoted to explore the vertical thermal conductivity of graphene paper. As shown in **Figure 6**a, Drzal and coworkers fabricated large-area freestanding graphene paper by vacuum filtration of graphene nanoplatelets.[100] The vacuum filtration and thermal annealing process could finely control the assembly and alignment of graphene nanosheets inside the paper structure (Figure 6b). The graphene paper exhibited a vertical thermal conductivity of 1.28 W m^{-1} K^{-1}, which was much lower than its in-plane heat conductivity (Figure 6c). As shown in Figure 6d,e, functionalized multilayer GO sheets were directionally and densely packed in graphene paper. As demonstrated in Figure 6f, this graphene paper prepared by vacuum filtration exhibited a distinct contrast between in-plane thermal conductivity and cross-plane thermal conductivity.[101] The former was up to 123 W m^{-1} K^{-1}, whereas the latter was only 1.81 W m^{-1} K^{-1}. In addition, as shown in Figure 6g–i, Li et al. successfully devised a lightweight and flexible composite paper by incorporating cellulose with GNPs.[102] The in-plane and cross-plane thermal conductivity of the robust composite paper with 75 wt% GNPs also showed significant differences; they were 59.46 and 0.64 W m^{-1} K^{-1}, respectively. Balandin and coworkers found that annealing of the freestanding GO paper at high temperature resulted in increasing the in-plane thermal conductivity and simultaneously reducing the cross-plane thermal conductivity.[103] In general, high-temperature annealing was an essential step in the preparation of graphene paper from GO, conducing the rearrangement of sp^{2}carbon and the removal of oxygen-containing functional groups, which further reduced the phonon scattering at the defects and functional groups, and finally resulted in the increase of in-plane thermal conductivity.[104] However, the decrease of the cross-plane thermal conductivity was attributed to the appearance of "air pockets" after high-temperature annealing, which induced a gap between the graphene layers, and further hindered smooth transmission of phonons in the vertical direction. All in all, relatively low thermal conductivity of graphene paper in the through-plane direction prevented its usage in high-performance TIMs. Thus, it can be seen that graphene paper may not be the best choice for direct construction of TIMs.

3.2.2. Randomly Arranged Graphene Composites for TIMs

In addition to graphene paper prepared from graphene sheet, a large amount of research has focused on the use of graphene-based composites for TIMs. Unlike the planar graphene paper, the graphene in the composite connected with each other to form a thermal conductive network in the vertical direction, thus improving the vertical thermal conductivity of composites. Significant effort was devoted to designing graphene-based composites for next-generation TIMs, including graphene–organic polymer resin composites (such as epoxies, urethanes, and silicones)[14,105–108] and graphene–inorganic thermal conductive filler composites (such as metals and ceramics).[7,13,109–111] It should be noted that the former composite contained only graphene and the polymer, while the latter was a binary–filler hybrid resin composition.

Polymer resins exhibited good processability and deformation, but unfortunately yielded an extremely low pristine thermal conductivity. Generally, graphene with high thermal conductivity was added into polymer resins to create composites with improved thermal conductivity.[105–107] Balandin and coworkers fabricated a dual-functional epoxy-based composite with the loading of 50 wt% of few-layer graphene fillers with a thickness of 12 nm.[14] **Figure 7**a,b is the photograph and SEM image of the composite, respectively. By finely regulating the thickness,

© 2020 Wiley-VCH GmbH

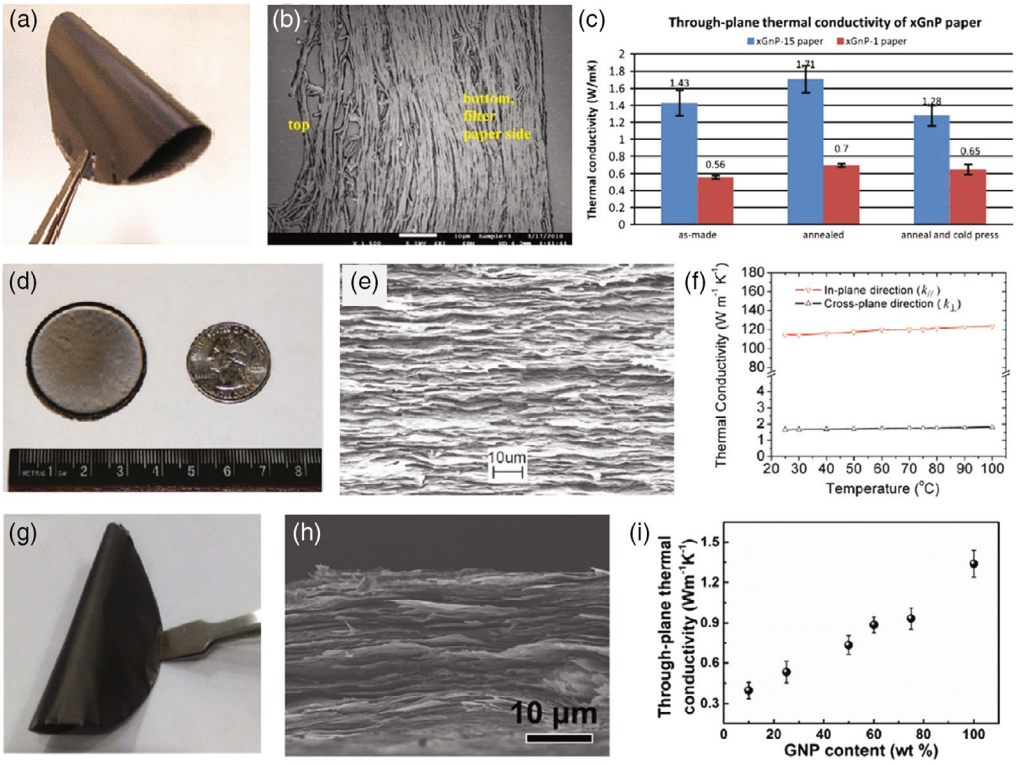

Figure 6. Planarly oriented graphene film for TIMs. a–c) Graphene paper fabricated by vacuum filtration of graphene nanoplatelets for TIMs, whose vertical thermal conductivity reached 1.28 W m^{-1} K^{-1}. Reproduced with permission.[100] Copyright 2011, Elsevier. d–f) Graphene paper prepared by vacuum filtration of functionalized multilayer GO sheets exhibiting a cross-plane thermal conductivity of 1.81 W m^{-1} K^{-1}. Reproduced with permission.[101] Copyright 2011, American Chemical Society. g–i) A composite paper successfully fabricated by mixing cellulose and GNPs yielded a cross-plane thermal conductivity of 0.64 W m^{-1} K^{-1}. Reproduced with permission.[102] Copyright 2017, Elsevier.

lateral dimensions, aspect ratio, and concentration of the graphene fillers, a dual-function composite with strong electromagnetic interference shielding and high vertical thermal conductivity properties was prepared. As shown in Figure 7c, the thermal conductivity of the composites increased as a function of the graphene fillers, reaching the value of 8 W m^{-1} K^{-1} when graphene filler loading was up to 55 wt%.

In addition to graphene being added as a filler into the resin, other inorganic materials with high thermal conductivity, such as graphite sheets, metals, and ceramics, have all been added as additives into the resin to enhance the vertical thermal conductivity of the resin matrix. As shown in Figure 7d,e, Lin et al. designed a porous graphene/ceramic composite by directly growing a graphene film on a porous ceramic for vertical heat transfer. The porous graphene/Al_2O_3 composite showed an interconnected framework and resulted in a thermal conductivity of 8.28 W m^{-1} K^{-1} (Figure 7f).[109] In addition, Goyal and Balandin studied the thermal properties of TIMs constructed by silver resin with hybrid graphene–metal particles as fillers. The vertical thermal conductivity of the TIMs reached 9.9 W m^{-1} K^{-1} at the small 5 vol% of graphene sheet loading in the silver resin.[111] Subsequently, they found that when the filler of graphene and multilayer graphene in the resin achieved a small loading of 2 vol%, the vertical thermal conductivity of the graphene-composite TIM reached 14 W m^{-1} K^{-1}.[7] A binary carbon filler is also a good choice to improve the vertical thermal conductivity of the polymer matrix. Yang and coworkers[112] and Yu and coworkers[113] fabricated graphene hybrid TIMs by self-assembly GO and high-quality graphene nanoplatelets. A low filler loading of graphene results in an unprecedented improvement in thermal conductivity of epoxy composites. To improve the insufficient conductive pathways and inefficient filler–filler contact, Fu and coworkers proposed to design a unique aggregated filler network by using graphene nanoplates and MWCNTs together.[110] Figure 7g,i shows a schematic diagram and a SEM image of a carbon nanotube (CNT)–graphene network, respectively. In this novel structure, filler–filler overlap can largely reduce the contact resistance, and MWCNTs embedded within the segregated graphene network increase the network density and improve the conductive pathways, and furthermore can enhance the thermal conductivity of this hybrid network. Balandin and coworkers put forward a statement of "synergistic filler effect."[13] The thermal properties of epoxy-based hybrid composites with graphene and CuNP fillers have been significantly improved to 13.5 ± 1.6 W m^{-1} K^{-1} (Figure 7l), which is attributed to the highly thermally conductive network formed by intercalation of spherical copper nanoparticles between the large graphene sheets (Figure 7j,k). This result demonstrates the potential of such hybrid epoxy composites for practical application in TIMs.

 © 2020 Wiley-VCH GmbH

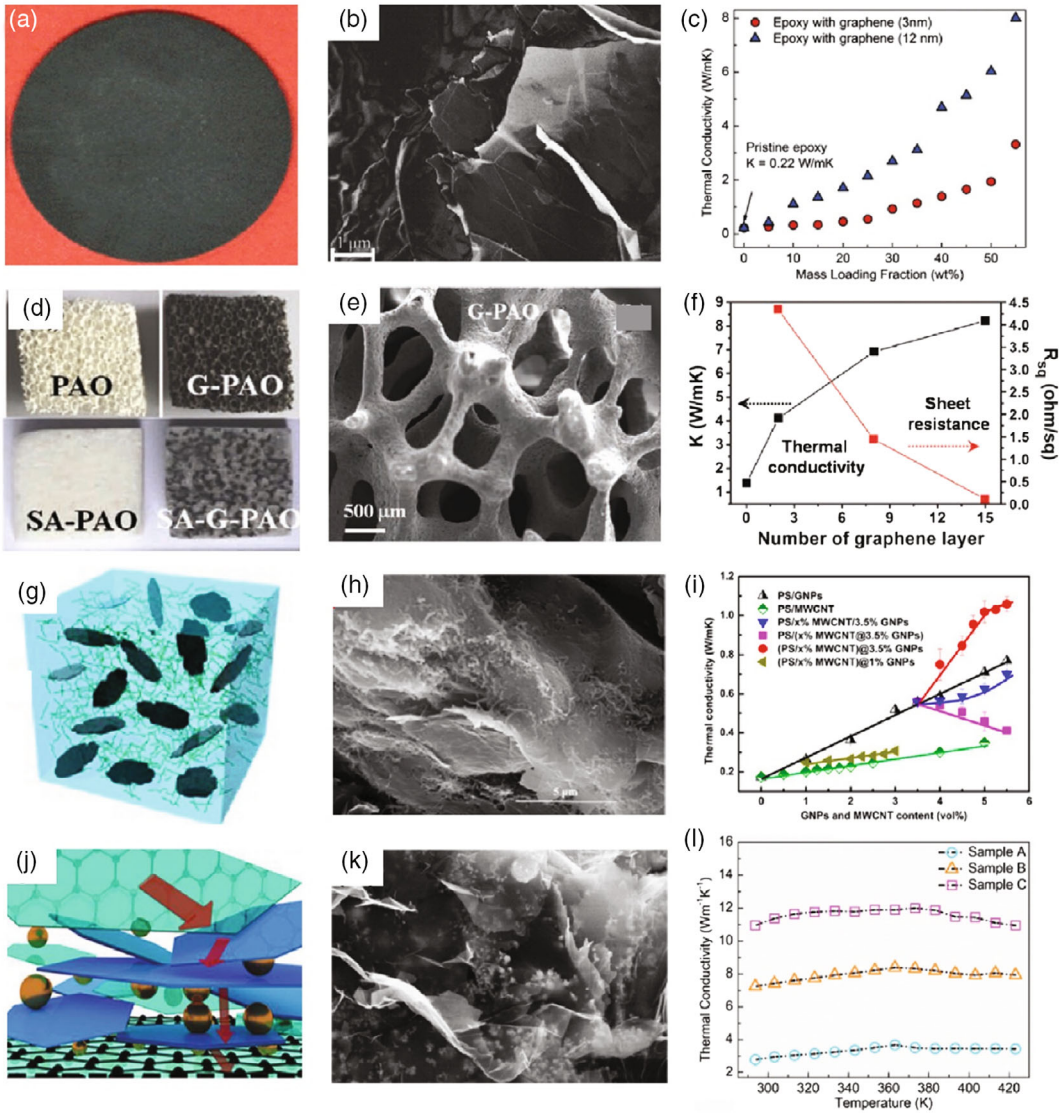

Figure 7. Randomly arranged graphene composites for TIMs. a–c) Graphene/resin composites for TIMs exhibited a vertical thermal conductivity of 8 W m^{-1} K^{-1}. Reproduced with permission.[14] Copyright 2019, Wiley-VCH. d–f) Porous graphene/ceramic composites for TIMs had a vertical thermal conductivity of 8.28 W m^{-1} K^{-1}. Reproduced with permission.[109] Copyright 2013, Wiley-VCH. g–i) A hybrid network was fabricated by mixing graphene nanoplates and multiwalled carbon nanotubes (MWCNTs) for TIMs. Reproduced with permission.[110] Copyright 2017, American Chemical Society. j–l) A "synergistic filler effect" statement was put forward. Graphene and copper nanoplates were synergistically added into the resin to increase thermal conductivity to 14 W m^{-1} K^{-1}. Reproduced with permission.[13] Copyright 2019, Wiley-VCH.

Although the thermal conductivity of graphene-based composites has been improved, the random alignment of graphene inevitably results in an increase in thermal contact resistance due to the loose contact between the graphene and resin surfaces. Therefore, vertical alignment of graphene sheets with thermal anisotropy is conducive to the vertical thermal conductivity of graphene-based TIMs.

3.2.3. Vertically Aligned Graphene Structure for TIMs

With the increasing demand for graphene-based TIMs with high thermal conductivity, compared with the random orientation of the graphene sheet, formation of a vertically aligned architecture of graphene is highly desirable to be achieved to break through the performance bottleneck of current TIMs. Recently, methods of preparing graphene materials with a vertical structure have been proposed gradually, which can be summarized as the top-down method and the bottom-up method. In the top-down method, TIMs are fabricated of VG structure by self-assembly GO or rGO sheets, whereas TIMs are directly constructed by as-grown VG in the bottom-up method. Subsequently, important advances in the preparation of TIMs by these two methods will be discussed in detail, respectively.

In the top-down method, the raw material for the preparation of TIMs is GO or rGO. To fully take advantage of the high in-plane thermal conductivity of graphene, GO or rGO sheets

 © 2020 Wiley-VCH GmbH

should be vertically aligned to form an efficient thermal conductance network along the vertical direction of TIMs. Park et al. demonstrated a high-performance polymer composite fabricated by melt compression of poly (vinylidene fluoride) (PVDF) and graphene nanoplates in an L-shape kinked tube.[114] Graphene fillers dispersed and directionally aligned in a polymer matrix, giving rise to a vertical thermal conductivity of $\approx 10\,W\,m^{-1}\,K^{-1}$ when the composite contained 25 vol% graphene nanoplates. Yu and coworkers demonstrated a highly efficient approach for improving the vertical thermal conductivity of polymer composites. **Figure 8**a,b shows highly anisotropic graphene aerogels (AGAs) with a vertically aligned graphene network, which were synthesized by directional freezing and freeze drying followed by high-temperature graphitization of the GO suspension.[25] Thermally annealed AGA (TAGA)/epoxy was fabricated using a vacuum-assisted impregnation method to mix TAGA with epoxy (Figure 8c). Due to the highly vertically oriented graphene structure, the TAGA/epoxy composite exhibited high vertical thermal conductivity of $6.57\,W\,m^{-1}\,K^{-1}$ with only 1.5 wt% TAGA (Figure 8d). Further research results showed that the thermal conductivity was linearly correlated with the directional-freezing rate. Low freezing rates during the freeze-drying process resulted in large pore structure, which in turn reduced the thermal conductivity of the composite structure. In addition, as shown in Figure 8e,f, Yu and coworkers devised vertically aligned graphene/GNP hybrid foams (GHFs) by hydrothermally treating a suspension of GO sheets in the presence of high-quality GNPs followed by air drying.[24] Figure 8g displays that the GHFs/epoxy composite exhibited the highest thermal conductivity when GNPs were added into the vertical thermal conductive network constructed by GO sheets. Moreover, the thermal conductivity of the GHF/epoxy composites increased with the annealing temperature. The thermal conductivity reached $35.5\,W\,m^{-1}\,K^{-1}$ when the annealing temperature was 2800 °C. The vertical thermal conductivity was signally improved when the graphene was aligned vertically even in polymer resins. However, the presence of a polymer resin can only increase the contact interface between the graphene powder and resin, so the phonon scattering was increased and the thermal conductivity was reduced. Instead of graphene powder dispersed in a polymer resin, Bai and coworkers proposed a novel method to fabricate graphene film–based resin composites, which combined a thermally reduced vertically aligned reduced graphene oxide (VArGO) film with epoxy resin.

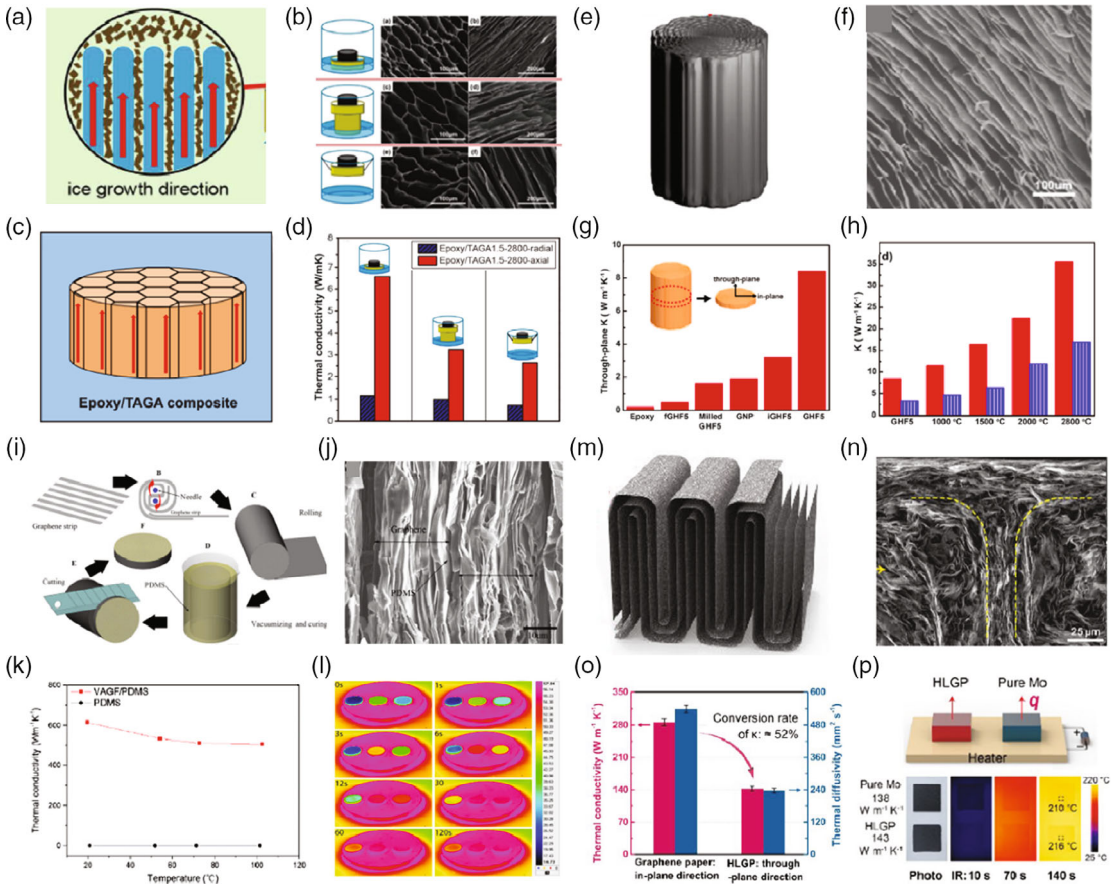

Figure 8. Vertically aligned graphene structure synthesized by top-down method for TIMs. a–d) Vertically aligned graphene aerogels synthesized by directional freezing for TIMs. Reproduced with permission.[25] Copyright 2018, Elsevier. e–h) Vertically aligned graphene/graphene nanoplatelet hybrid aerogels prepared by hydrothermal reaction followed by air drying for TIMs. Reproduced with permission.[24] Copyright 2018, American Chemical Society. i–l) Vertically aligned graphene films rolled up the tailored GO films for TIMs. Reproduced with permission.[21] Copyright 2016, Elsevier. m–p) VG monoliths formed by shrinking–compressing graphene paper for TIMs. Reproduced with permission.[16] Copyright 2019, American Chemical Society.

© 2020 Wiley-VCH GmbH

This method mainly involved the fabrication of an rGO/polyvinyl alcohol (PVA) composite film and fabrication of a thermally reduced VArGO/PVA composite. A well-dispersed GO aqueous solution was coated on zinc foil surface and then thermally reduced to form the rGO film, which was then impregnated into the PVA solution and dried to obtain the rGO/PVA composite film. The composite film was cut into strips, which were then rolled up to form a graphene-based TIM with a vertical structure. The thermal conductivity of the vertical rGO was up to 2.645 $W\,m^{-1}\,K^{-1}$ and the thermal conductivity enhancement was as high as 887%.[20] Later, as shown in Figure 8i, they tailored purchased graphene films with thickness of 25 mm into narrow strips, which were rolled to form a cylinder with a diameter of about 12.7 mm. After dipping into polydimethylsiloxane (PDMS) and vacuum drying, the cylinder was cut into desired thickness for construction of TIMs. PDMS serves as the adhesive to keep graphene films tightly stacked together, while vertically aligned graphene films (VAGFs) provide enough mechanical strength to the composite, which endows the VAGF/PDMS composite with excellent mechanical properties and ultrahigh thermal conductivity of 614.85 $W\,m^{-1}\,K^{-1}$ (Figure 8k,l).[21] Using the same physical-mechanical machining method on graphene paper, Lin and coworkers designed a honeycomb panel–like graphene pad (HLGP) with a vertical structure by shrinking–compressing graphene paper for TIM application (Figure 8m).[16] When applying a specific lateral mechanical force to the planarly stacked graphene paper, a vertically aligned graphene architecture could be obtained, as shown in Figure 8n. As demonstrated in Figure 8o, after the graphene structural transformation from horizontal to vertical orientation, the VG monoliths still exhibited a high out-of-plane thermal conductivity of 143 $W\,m^{-1}\,K^{-1}$. Subsequently, comparative tests between graphene and molybdenum proved that HLPG had better vertical thermal conductivity, suggesting that HLPG has more potential to be used for TIMs.

In the top-down method, GO dispersion or graphene paper is used to construct TIMs, while in the bottom-up method, TIM is prepared by directly growing VG. The synergy of the superior inherent properties of graphene and the special structural endows vertical attractive thermal properties. As shown in **Figure 9**a, Liu and coworkers used DC-PECVD to grow VG at a height of several tens of nanometers directly on a sapphire substrate, which acts as a nucleation site for the growth of aluminum nitride (AlN).[17] Standing between the sapphire and the aluminum nitride interface, the VG can be regarded as a TIM to transfer heat. The vertical thermal conductivity of the VG buffer layer measured with the traditional Raman method was up to 680 $W\,m^{-1}\,K^{-1}$, which is the highest vertical thermal conductivity so far. Excellent thermal conductivity of VG promoted heat dissipation between the AlN film and a sapphire substrate in the vertical direction (Figure 9b). Benefiting from the excellent thermal conductivity of VG for effective heat dissipation, high-performance InGaN-based ultraviolet light-emitting diodes devices exhibit high brightness and high efficiency. For rapid growth of higher VG, whose thermal conductivity may be accurately tested without the substrate interference, Zhang et al. adopted an alcohol-based electric-field-assisted PECVD method (Figure 9c) to prepare VG arrays with a height of 18.7 μm, which were completely perpendicular to the substrates (Figure 9d). The orderly arrangement of the fully erected sheets endowed the VG arrays with excellent thermal properties, and they exhibited a high vertical thermal conductivity of 53.5 $W\,m^{-1}\,K^{-1}$ and a low contact thermal resistance of 11.8 $K\,mm^2\,W^{-1}$, which were measured by the time-domain thermoreflectance method and steady-state thermal flow methods, respectively.[12] To evaluate the potential of the VG arrays as TIMs in electronic devices, a test system was designed to simulate heat dissipation in electronic components. The VG-based TIM is displayed in Figure 9e; it can significantly reduce the operating temperature of power devices compared with thermal conductive tape and graphene nanowall–based TIMs, as shown in Figure 9f. Higher VG is not only beneficial for more accurate measurement of vertical thermal conductivity, but also promotes more efficient interfacial heat transfer. In addition, it is noteworthy that Cen and coworkers proposed to construct tree-inspired radially aligned, bimodal graphene frameworks for highly efficient thermal transport.[115] Although a radially aligned graphene skeleton serves as the primary pathway for heat conduction, tree-leaf-like graphene vertically grown on the graphene skeleton plays a crucial role in providing additional thermal pathways for phonon transportation, which can

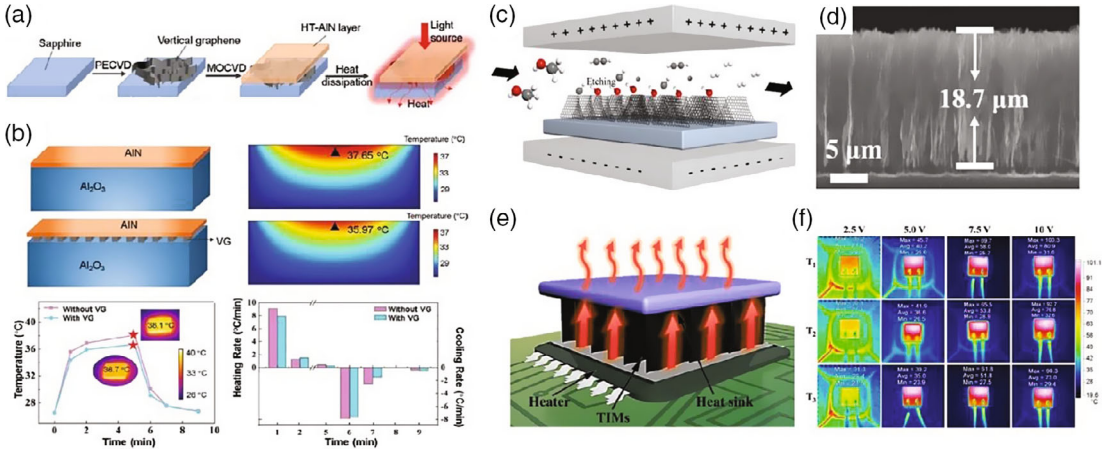

Figure 9. VG prepared by bottom-up method for TIMs. a,b) VG grown by DC-PECVD for heat dissipation of LED. Reproduced with permission.[17] Copyright 2019, Wiley-VCH. c–f) VG arrays grown with AEF-PECVD for TIM application. Reproduced with permission.[12] Copyright 2020, Wiley-VCH.

 © 2020 Wiley-VCH GmbH

promote the heat dissipation of the whole radial skeleton. These innovative works suggest that preparing aligned and erect graphene is of crucial importance for realizing efficient heat transfer in TIMs, which is of great promise for the practical thermal management of electronic and energy storage devices.

3.3. The Evolution of Graphene-Based TIMs

As mentioned previously, graphene and graphene derivatives have been widely investigated for building graphene-based TIMs over recent years. Originally, the unique graphene paper assembled of microscopic graphene sheet building blocks was regarded as alternate material for TIM application. Soon after, the well-developed graphene–resin composites were widely adopted in TIMs. Especially, graphene–metal or graphene–ceramic as synergetic fillers have endowed newly designed resin-based TIMs with excellent thermal conductivity. Recently, emerging physical mechanical machining techniques and chemical vapor deposition have been explored to prepare VG with high thermal conductivity for applications of TIMs in multifunctional power devices.

As shown in **Figure 10**, from 2011 up to the present, considerable effort has been devoted to preparing graphene-based TIMs with high thermal conductivity. At the early stage, people tried using graphene paper to transfer heat vertically. The graphene paper prepared by vacuum filtration or the dip-coating method yielded excellent in-plane thermal conductivity, due to the formation of a continuous planar thermal conductive network by tightly self-assembling layers of GO sheets. However, functional groups or defects present on the graphene surface, together with the weak Van der Waals force and π–π interactions between layer and layer, frustrate phonon transport in the vertical direction, eventually leading to low vertical thermal conductivity of graphene paper. Figure 10 (in gray) shows some typical works of graphene paper used for TIMs. The vertical thermal conductivity of graphene paper could reach up to 1.81 $W\,m^{-1}\,K^{-1}$, which is difficult to satisfy the requirements of TIMs.[101]

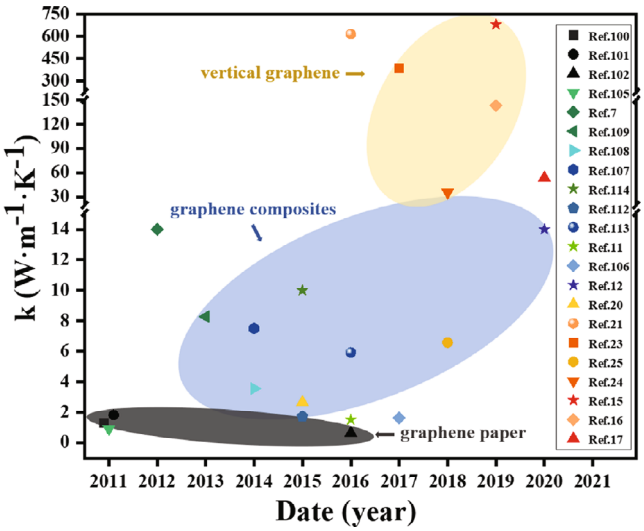

Figure 10. The development of graphene-based TIMs and their vertical thermal conductivity. By designing different structures of graphene-based TIMs, different thermal conductivities could be obtained. After all, the assembly method decides the specific structure of graphene-based TIMs, and the special design of TIMs' structure determines their excellent thermal property.

Meanwhile, with an increasing concern on improvement of the vertical thermal conductivity of TIMs, it occurred to researchers that directly forming a VG-based network would be beneficial for vertical heat transfer. As shown in Figure 10 (in blue), a great deal of attention were paid to building graphene–resin composites by mixing graphene powder with a polymer resin for TIM applications. This method was widely used in industry and laboratories due to its relatively simple experimental process, combined with a large variety of potential filler candidates. Graphene sheets could couple with the matrix material as a separate filler, due to their high thermal conductivity and mechanical flexibility. Below the thermal percolation threshold, the thermal conductivity of the graphene–resin composites was positively correlated with the loading capacity of the graphene fillers. However, excessive graphene fillers induced the agglomeration of graphene powder, resulting in viscosity and uniformity of the graphene–resin composites. By fine-tuning the size distribution and dispersion of the graphene sheets, the vertical thermal conductivity of a graphene–resin composite was effectively increased to ≈10 $W{\cdot}m^{-1}{\cdot}K^{-1}$.[14] To further improve the thermal conductivity of composites, fillers with high thermal conductivity, such as metals, ceramics, graphite plate, and CNTs, together with graphene were added into the polymer resin matrix. Synergistic size-dissimilar fillers provide efficient filler−filler contact and sufficient conductive pathways for a strong enhancement of the thermal conductivity of composites, which could reach ≈15 $W\,m^{-1}\,K^{-1}$.[13] In graphene–resin composites, fillers contact with each other in small areas, which reduces the interfacial thermal resistance to some extent and further results in the relatively finite enhancement of thermal conductivity, because a large interfacial thermal resistance still exists between synergistic fillers. Moreover, the random alignment of graphene sheets in a polymer matrix, together with loose contact between graphene and the resin or additives, tends to restrain the excellent thermal conductance of a hybrid graphene network. Therefore, only limited enhancement of thermal conductivity has been observed in graphene–resin composites composed of a randomly dispersed graphene–resin hybrid network, which indicates that it is not only the type and amount of fillers but also the orientation of the conductive network that matters.

In recent years, some research has gradually explored vertically erect graphene sheets to form an efficient thermal conductance network along the vertical direction of TIMs, fully taking advantage of the high in-plane thermal conductivity of graphene. In terms of the preparation method, it could be classified into a top-down method and a bottom-up method. The top-down approach involves two different strategies. One strategy is dealing with the dispersion solution of GO and resin, which plays an important role in constructing a vertically aligned interconnection network. Directional freezing followed by freeze drying and hydrothermal reduction followed by air drying both have been widely used to construct anisotropic graphene foams with GO liquid crystals as building blocks. The directional arrangement of GO sheets gave the as-prepared graphene foams a vertical thermal conductive network, thus endowing the vertically

© 2020 Wiley-VCH GmbH

oriented graphene foams with high vertical thermal conductivity. The thermal conductivity of the VG structure prepared with this strategy was increased to 35.5 W m^{-1} K^{-1}.[24] The other strategy is to manipulate graphene paper. Rolling–cutting and shrinking–compressing are typical methods for building VG structures using graphene paper. In general, graphene paper was formed by self-assembly of graphene sheets. In the process of erecting graphene paper into a VG structure, the in-plane thermal conductivity effectively reserved in graphene paper was transformed into the vertical thermal conductivity of a VG structure. Therefore, whether the VG films were constructed by rolling up cut graphene strips or the VG monolith was prepared by applying a horizontal mechanical force to stacked graphene paper, both showed excellent vertical thermal properties. In particular, the thermal conductivity of VG prepared by the rolling–cutting method reached 614.85 W m^{-1} K^{-1}, which is the highest vertical thermal conductivity of graphene prepared by the top-down method[21] In addition to the mechanical methods, VG can also be grown directly by PECVD, which is a typical bottom-up method to prepare graphene-based TIMs. By changing the growth conditions, the layer number and height of graphene can be controlled so that the thermal properties of as-grown VG are closer to the intrinsic properties of graphene. Thus, TIMs directly constructed by as-grown VG exhibited remarkable thermal properties. The highest point in Figure 10 is the thermal conductivity of VG prepared by the PECVD method, which could reach up to 680 W m^{-1} K^{-1}.[17] This unprecedented result is also the highest reported thermal conductivity for a graphene material so far.

From planar graphene paper with no vertical orientation to VG with a specially designed structure, graphene-based TIMs are constantly being updated. In Figure 10, with the continuous breakthrough in the vertical thermal conductivity of graphene materials, we can notice the development trend of graphene-based TIMs. Two important conclusions can be drawn from this development process. One is that the vertical alignment of graphene is crucial for improving the vertical thermal conductivity of graphene-based TIMs. From 2011 to 2020, the vertical thermal conductivity of graphene materials appeared as an upward trend, accompanied by the random orientation of graphene composites replacing the planar graphene films and then being replaced by the vertical structure of graphene. The other is that direct growth of VG with PECVD has great potential in the preparation of graphene-based TIMs, which is yielding the highest vertical thermal conductivity now. Growing graphene by PECVD is a one-step process compared to other preparation methods. In other methods, GO is used as the raw material. The dry preparation process involves the formation of a GO dispersion solution, obtainment of GO films, erection of GO paper, together with reduction and annealing of vertical rGO structure, while the wet process involves the formation of a GO dispersion solution, mixing of graphene and polymers or other fillers, curing and molding of graphene composites, as well as reduction and annealing of the VG structure. However, the VG can be grown directly after the instrument procedures and reaction conditions are accurately set when using PECVD. In addition, the morphology and growth rate of VG can be precisely controlled by reaction parameters in PECVD. More importantly, as-grown VG can be directly used as TIM without any aid of polymers or other fillers. Phonons can spread directly along the graphene sheets, avoiding phonon scattering at the interface between graphene and the polymer. In other methods, graphene powders were overlapped with each other to form a thermal conductive network, requiring a polymer or other fillers to fill the graphene skeleton and consolidate the graphene structure. Phonon scattering at the boundary of the graphene sheets and the contact interfaces between graphene and the polymer seriously hinder the smooth transmission of phonons in the graphene structure, so there is only limited thermal conductivity in these composite VG materials. Compared with graphene self-assembly, the properties of directly grown VG are closer to the intrinsic properties of graphene; therefore, it exhibits higher thermal properties. In short, Figure 10 shows us the direction for the preparation of high-performance TIMs. The construction of a VG structure is crucial for the improvement of the vertical thermal conductivity of graphene materials. In particular, VG grown through PECVD is the best choice for the construction of graphene-based TIMs.

4. Conclusion

This review serves as a critical analysis and summary of the state of the art of the VG from fabrication to final TIMs applications. With the demand for high-performance TIMs in electronic devices, planarly oriented graphene paper, randomly arranged graphene composites, and vertically aligned graphene materials have been gradually developed. Graphene materials with a vertical structure have been proven to act as the most efficient TIMs, as the VG structure effectively accelerates phonon transport in the vertical direction, naturally increasing the vertical thermal conductivity of the VG-based TIMs. Nevertheless, to transfer the intrinsic properties of graphene to the macroscopic VG-based TIMs, the graphene assembly methods are very critical. Based on this, the top-down method represented by physical-mechanical method and the bottom-up method represented by PECVD method have been rapidly developed. At the same time, VG materials such as VG aerogels, VG monoliths, and VG arrays have been increasingly used as TIMs. By comparing the thermal conductivity of VG structures prepared by different methods, it can be found that the VG prepared by PECVD as TIM yields the highest thermal conductivity at present, showing great heat dissipation potential.

By using PECVD, VG can be grown on a wide range of substrates at low temperatures without using catalysts. The morphology and properties of VG can be controlled by changing PECVD parameters during growth. However, different types of PECVD exhibit different characteristics to prepare VG with different growth rates and morphologies. In this review, we summarize and analyze some typical reported works on the morphology and growth rate of graphene. In the process of growing VG with PECVD, the growth rate and morphology of VG are affected by many factors, which makes the growth process of VG very complicated. Although the interpretation of the controllable growth process of VG remains elusive and puzzling, a consistent and widely accepted mechanism for nucleation and growth is extensively studied. Further study of the growth mechanism will not only help explain the experimental results in the complex plasma growth reaction, but also hopefully guide us to accurately control the morphology and properties of VG.

© 2020 Wiley-VCH GmbH

Table 2. Key parameters to evaluate TIMs.

Method	Material	Thermal conductivity [W m^{-1} K^{-1}]	Thermal resistance [K mm^2 W^{-1}]	Young's modulus [MPa]	Compression strength [MPa]	Cost
Top-down	graphene nanoflakes[114]	10	–	–	–	–
	rGO/epoxy composite[20]	2.65	–	–	–	–
	VAGF[21]	614.86	–	86.023	2.255	–
	GF/E-40[23]	384.9	–	910.77	12.33	–
	AGAs[25]	6.57	–		20/150	–
	GHF-2800[24]	35.5	–	406	–	–
	HLGP[16]	143	5.8–22.5	–	0.87	–
Bottom-up	VG arrays[12]	53.5	11.8	–	–	–
	VG[17]	680	–	–	–	–

Direct growth of VG by PECVD has been demonstrated to be the best strategy to extend the intrinsic properties of graphene to macro graphene-based TIMs. In VG arrays grown by PECVD, the graphene sheets are neatly arranged and completely perpendicular to the growth substrates, which is conducive to a significant increase in vertical thermal conductivity. Although as-grown VG with high thermal conductivity has shown distinct advantages in TIMs, only limited works have been reported on growing VG for TIM applications. Therefore, more effort needs to be devoted for the growth of VG with excellent thermal properties. The research would have been more persuasive if more VG-array-based TIMs had been explored. Structure determines properties. More specifically, the morphology and height of VG are bound to affect the thermal properties of graphene-based TIMs. However, the effect of VG structure on the thermal properties of TIMs has not been thoroughly studied. A large number of experiments are needed to investigate the effect of the morphology of VG on the properties of TIMs, such as thermal conductivity and contact thermal resistance.

When it comes to interfacial contact thermal resistance, as one of the evaluation criteria for the thermal properties of graphene-based TIMs, it has not been taken into account in plenty of works. As shown in **Table 2**, when making a general survey of the current studies on graphene-based TIMs, we can find that thermal conductivity was studied in each work, while a limited number of works focused on contact thermal resistance and only a small number of works focused on the mechanical properties of TIMs. However, in addition to thermal conductivity, interface contact thermal resistance is equally critical to evaluate the performance of TIMs. As the vertical thermal conductivity of the VG structure reaches a certain high value, the thermal resistance of TIMs will mainly be produced from the contact interface. Naturally, in this case, the interface thermal resistance has a huge impact on the performance of TIMs. Thus, it can be seen that TIMs with excellent performance not only need to transfer heat effectively, but also need to be in good contact with the heater and the heat sink. In future studies, the thermal properties of TIMs, including thermal conductivity and thermal resistance, should be evaluated more comprehensively. In addition to the thermal properties, all key parameters such as the mechanical behavior, adaptability, and even the cost should be evaluated.

Of course, in addition to considering the relationship between the preparation method and the thermal properties of VG, the feasibility of the preparation method for mass production of VG should also be seriously considered. Currently, commercial graphene-based TIMs are actually graphene–resin composites. Mixing graphene and a polymer resin enables the mass production of graphene-based TIMs, which is attributed to the rapid mass production of graphene. However, the vertical thermal conductivity of graphene composites has maintained at only $\approx$10 W m^{-1} K^{-1}, with which it is difficult to meet the current demands of integrated high-power devices. PECVD can directly grow VG with high thermal conductivity, but the inevitable problem is mass production. We know that over the past decade, mass production of graphene films through roll-to-roll CVD has been realized. Therefore, we can learn from the mature growth methods of graphene films, optimize the growth process, improve the growth equipment, and create possibilities for the mass growth of VG.

All in all, graphene's excellent thermal conductivity makes it a promising candidate for thermal management. In particular, VG with special morphology can be used as a high-performance TIM, which is expected to effectively solve the heat dissipation problem of electronic devices. The outstanding thermal properties of VG will encourage and inspire additional studies on the design and preparation of VG-based TIMs. In the process of assembling nanoscale graphene sheets into macro thermal conductive materials, maintaining and extending the excellent thermal properties of graphene is the core problem facing the large-scale preparation and application of graphene in the field of thermal management. Only through continuous innovation of assembly strategy and optimization of the preparation process can graphene materials become practical TIMs that can be widely used.

Acknowledgements

The authors thank Yangyong Sun and Shanshan Wang from Peking University for their kind suggestion and discussion on the review. This research was financially supported by the Ministry of Science and Technology of China (2016YFA0200101), the National Natural Science Foundation of China (Grant No. 51720105003), and Beijing National Laboratory for Molecular Sciences (BNLMS- CXTD-202001).

 © 2020 Wiley-VCH GmbH

Conflict of Interest

The authors declare no conflict of interest.

Keywords

heat dissipation, plasma enhanced chemical vapor deposition, thermal interface materials, vertical graphene

Received: July 8, 2020
Published online:

[1] D. Cahill, P. Braun, G. Chen, D. R. Clarke, S. H. Fan, K. E. Goodson, P. Keblinski, W. P. King, G. D. Mahan, A. Majumdar, H. J. Maris, S. R. Phillpot, E. Pop, L. Shi, *Appl. Phys. Rev.* **2014**, *1*, 011305.
[2] A. L. Moore, L. Shi, *Mater. Today* **2014**, *17*, 163.
[3] J. Schleeh, J. Mateos, N. W. I. Iniguez-de-la-Torre, P. A. Nilsson, J. Grahn, A. J. Minnich, *Nat. Mater.* **2015**, *14*, 187.
[4] S. Naghibi, F. Kargar, D. Wright, C. Y. T. Huang, A. Mohammadzadeh, Z. Barani, R. Salgado, A. A. Balandin, *Adv. Electron. Mater.* **2020**, *6*, 1901303.
[5] A. P. Yu, P. Ramesh, M. E. Itkis, E. Bekyarova, R. C. Haddon, *J. Phys. Chem. C* **2007**, *111*, 7565.
[6] A. A. Balandin, *Nat. Mater.* **2011**, *10*, 569.
[7] K. M. Shahil, A. A. Balandin, *Nano Lett.* **2012**, *12*, 861.
[8] J. Hansson, T. M. J. Nilsson, L. L. Ye, J. Liu, *Int. Mater. Rev.* **2019**, *63*, 22.
[9] E. Pop, V. Varshney, A. K. Roy, *MRS Bull.* **2012**, *37*, 1273.
[10] A. A. Balandin, S. Ghosh, W. Bao, I. Calizo, D. Teweldebrhan, F. Miao, C. N. Lau, *Nano Lett.* **2008**, *8*, 902.
[11] X. Shen, Z. Wang, Y. Wu, X. Liu, Y. B. He, J. K. Kim, *Nano Lett.* **2016**, *16*, 3585.
[12] S. C. Xu, S. S. Wang, Z. Chen, Y. Y. Sun, Z. F. Gao, H. Zhang, J. Zhang, *Adv. Funct. Mater.* **2020**, *30*, 2003302.
[13] Z. Barani, A. Mohammadzadeh, A. Geremew, C. Y. Huang, D. Coleman, L. Mangolini, F. Kargar, A. A. Balandin, *Adv. Funct. Mater.* **2019**, *30*, 1904008.
[14] F. Kargar, Z. Barani, M. Balinskiy, A. S. Magana, J. S. Lewis, A. A. Balandin, *Adv. Electron. Mater.* **2019**, *5*, 1904008.
[15] Z. Wu, C. Xu, C. Ma, Z. Liu, H. Cheng, W. Ren, *Adv. Mater.* **2019**, *31*, 1900199.
[16] W. Dai, T. Ma, Q. Yan, J. Gao, X. Tan, L. Lv, H. Hou, Q. Wei, J. Yu, J. Wu, Y. Yao, S. Du, R. Sun, N. Jiang, Y. Wang, J. Kong, C. Wong, S. Maruyama, C. T. Lin, *ACS Nano* **2019**, *13*, 11561.
[17] H. Ci, H. Chang, R. Wang, T. Wei, Y. Wang, Z. Chen, Y. Sun, Z. Dou, Z. Liu, J. Li, P. Gao, Z. Liu, *Adv. Mater.* **2019**, *31*, e1901624.
[18] X. H. Li, P. F. Liu, X. F. Li, F. An, P. Min, K. N. Liao, Z. Z. Yu, *Carbon* **2018**, *126*, 119.
[19] Y. Yoon, K. Lee, S. S. S. Kwon, H. Yoo, S. J. Kim, Y. H. Shin, Y. H. Park, D. Kim, J. Choi, H. Lee, *ACS Nano* **2015**, *8*, 4580.
[20] D. Han, Y. H. Zhao, Y. F. Zhang, S. L. Bai, *RSC Adv.* **2015**, *5*, 94426.
[21] Y. F. Zhang, D. Han, Y. H. Zhao, S. L. Bai, *Carbon* **2016**, *109*, 552.
[22] G. Lian, C. C. Tuan, L. Li, S. Jiao, Q. Wang, K. S. Moon, D. Cui, C. P. Wong, *Chem. Mater.* **2016**, *28*, 6096.
[23] Y. F. Zhang, Y. J. Ren, S. L. Bai, *Int. J. Heat Mass Transfer* **2018**, *118*, 510.
[24] F. An, X. F. Li, P. Min, P. F. Liu, Z. G. Jiang, Z. Z. Yu, *ACS Appl. Mater. Interfaces* **2018**, *10*, 17383.
[25] X. Li, P. F. Liu, X. F. Li, F. An, P. Min, K. N. Liao, Z. Z. Yu, *Carbon* **2018**, *140*, 624.
[26] F. Guo, A. Mukhopadhyay, B. W. Sheldon, R. H. Hurt, *Adv. Mater.* **2011**, *23*, 508.
[27] J. Renteria, S. Legedza, R. Salgado, M. P. Balandin, S. Ramirez, M. Saadah, F. Kargar, A. A. Balandin, *Mater. Des.* **2015**, *88*, 214.
[28] W. Liu, T. Dang, Z. Xiao, X. Li, C. Zhu, X. Wang, *Carbon* **2011**, *49*, 884.
[29] K. Yu, G. Lu, Z. Bo, S. Mao, J. Chen, *J. Phys. Chem. Lett.* **2011**, *2*, 1556.
[30] K. Yu, P. Wang, G. Lu, K. H. Chen, Z. Bo, J. H. Chen, *J. Phys. Chem. Lett.* **2011**, *2*, 537.
[31] Z. Bo, Z. Wen, H. Kim, G. h. Lu, K. H. Yu, J. H. Chen, *Carbon* **2012**, *50*, 4379.
[32] J. Zhao, M. Shaygan, J. Eckert, M. Meyyappan, M. H. Rummeli, *Nano Lett.* **2014**, *14*, 3064.
[33] K. Davami, M. Shaygan, N. Kheirabi, J. Zhao, D. A. Kovalenko, M. H. Rümmeli, J. Opitz, G. Cuniberti, J. Lee, M. Meyyappan, *Carbon* **2014**, *72*, 372.
[34] M. Zhu, J. Wang, B. C. Holloway, R. A. Outlaw, X. Zhao, K. Hou, V. Shutthanandan, D. M. Manos, *Carbon* **2007**, *45*, 2229.
[35] M. Cai, R. A. Outlaw, S. M. Butler, J. R. Miller, *Carbon* **2012**, *50*, 5481.
[36] C. H. Tu, W. Chen, H. C. Fang, Y. Tzeng, C. P. Liu, *Carbon* **2013**, *54*, 234.
[37] M. Hiramatsu, Y. Nihashi, H. Kondo, M. Hori, *Jpn. J. Appl. Phys.* **2013**, 52.
[38] J. Shan, L. Cui, F. Zhou, R. Wang, K. Cui, Y. Zhang, Z. Liu, *ACS Appl. Mater. Interfaces* **2020**, *12*, 11972.
[39] A. T. H. Chuang, B. O. Boskovic, J. Robertson, *Diamond Relat. Mater.* **2006**, *15*, 1103.
[40] Y. H. Wu, T. Yu, Z. X. Shen, *J. Appl. Phys.* **2010**, *108*, 071301.
[41] S. Mori, T. Ueno, M. Suzuki, *Diamond Relat. Mater.* **2011**, *20*, 1129.
[42] K. H. Yu, Z. Bo, G. H. Lu, S. Mao, S. M. Cui, Y. W. Zhu, X. Q. Chen, R. S. Ruoff, J. H. Chen, *Nanoscale Res. Lett.* **2011**, *6*, 202.
[43] D. C. Wei, L. Peng, M. Li, H. Mao, T. Niu, C. Han, W. Chen, A. T. S. Wee, *ACS Nano* **2015**, *9*, 164.
[44] G. Sato, T. Morio, T. Kato, R. Hatakeyama, *Jpn. J. Appl. Phys.* **2006**, *45*, 5210.
[45] S. Vizireanu, S. D. Stoica, C. Luculescu, L. C. Nistor, B. Mitu, G. Dinescu, *Plasma Sources Sci. Technol.* **2010**, *19*, 034016.
[46] K. Shiji, M. Hiramatsu, A. Enomoto, M. Nakamura, H. Amano, M. Hori, *Diamond Relat. Mater.* **2005**, *14*, 831.
[47] S. Kondo, M. Hori, K. Yamakawa, S. Den, H. Kano, M. Hiramatsu, *J. Vac. Sci. Technol. B* **2008**, *26*, 1294.
[48] L. Y. Zeng, D. Lei, W. B. Wang, J. Q. Liang, Z. Q. Wang, N. Yao, B. L. Zhang *Appl. Surf. Sci.* **2008**, *254*, 1700.
[49] Z. Bo, Y. Yang, J. Chen, K. Yu, J. Yan, K. Cen, *Nanoscale* **2013**, *5*, 5180.
[50] Z. Bo, S. Mao, Z. J. Han, K. Cen, J. Chen, K. K. Ostrikov, *Chem. Soc. Rev.* **2015**, *44*, 2108.
[51] Z. Y. Zhang, C. S. Lee, W. J. Zhang, *Adv. Energy Mater.* **2017**, *7*, 1700678.
[52] S. Kurita, A. Yoshimura, H. Kawamoto, T. Uchida, K. Kojima, M. Tachibana, P. Molinamorales, H. Nakai, *J. Appl. Phys.* **2005**, *97*, 104320.
[53] Q. Q. Kong, Z. Liu, J. G. Gao, C. M. Chen, Q. Zhang, G. Zhou, Z. C. Tao, X. H. Zhang, M. Z. Wang, F. Li, R. Cai, *Adv. Funct. Mater.* **2014**, *24*, 4222.
[54] H. Ci, H. Ren, Y. Qi, X. Chen, Z. Chen, J. Zhang, Y. Zhang, Z. Liu, *Nano Res.* **2018**, *11*, 3106.
[55] Y. Zhang, J. Du, S. Tang, P. Liu, S. Deng, J. Chen, N. Xu, *Nanotechnology* **2012**, *23*, 015202.
[56] K. Tanaka, M. Yoshimura, A. Okamoto, K. Ueda, *Jpn. J. Appl. Phys.* **2005**, *44*, 2074.
[57] Y. Zhang, Q. Zou, H. S. Hsu, S. Raina, Y. Xu, J. B. Kang, J. Chen, S. Deng, N. Xu, W. P. Kang, *ACS Appl. Mater. Interfaces* **2016**, *8*, 7363.
[58] N. G. Shang, P. Papakonstantinou, M. McMullan, M. Chu, A. Stamboulis, A. Potenza, S. S. Dhesi, H. Marchetto, *Adv. Funct. Mater.* **2008**, *18*, 3506.

 © 2020 Wiley-VCH GmbH

[59] A. Malesevic, R. Vitchev, K. Schouteden, A. Volodin, L. Zhang, G. V. Tendeloo, A. Vanhulsel, C. V. Haesendonck, *Nanotechnology* **2008**, *19*, 305604.
[60] K. Teii, S. Shimada, M. Nakashima, A. T. H. Chuang, *J. Appl. Phys.* **2009**, *106*, 084303.
[61] W. Takeuchi, M. Ura, M. Hiramatsu, Y. Tokuda, H. Kano, M. Hori, *Appl. Phys. Lett.* **2008**, *92*, 213103.
[62] T. M. Dinh, A. Achour, S. Vizireanuc, G. Dinescuc, L. Nistord, K. Armstronge, D. Guaye, D. Pech, *Nano Energy* **2014**, *10*, 288.
[63] M. Hiramatsu, K. Shiji, H. Amano, M. Hori, *Appl. Phys. Lett.* **2004**, *84*, 4708.
[64] J. Wang, M. Zhu, R. A. Outlaw, X. Zhao, D. M. Manos, B. C. Holloway, *Carbon* **2004**, *42*, 2867.
[65] M. Y. Zhu, R. A. Outlaw, M. Bagge-Hansen, H. J. Chen, D. M. Manos, *Carbon* **2011**, *49*, 2526.
[66] C. Yang, H. Bi, D. Wan, F. Huang, X. Xie, M. Jiang, *J. Mater. Chem. A* **2013**, *1*, 770.
[67] Y. Ma, H. Jang, S. J. Kim, C. Pang, H. Chae, *Nanoscale Res. Lett.* **2015**, *10*, 1019.
[68] Y. Ma, W. Jiang, J. Han, Z. Tong, M. Wang, J. Suhr, X. Chen, L. Xiao, S. Jia, H. Chae, *ACS Appl. Mater. Interfaces* **2019**, *11*, 10237.
[69] S. Wu, S. Peng, Z. J. Han, H. Zhu, C. H. Wang, *ACS Appl. Mater. Interfaces* **2018**, *10*, 36312.
[70] S. Huang, G. He, C. Yang, J. Wu, C. Guo, T. Hang, B. Li, C. Yang, D. Liu, H. J. Chen, Q. Wu, X. Gui, S. Deng, Y. Zhang, F. Liu, X. Xie, *ACS Appl. Mater. Interfaces* **2019**, *11*, 1294.
[71] S. Ghosh, S. R. Polaki, M. Kamruddin, S. M. Jeong, K. Ostrikov, *J. Phys. D Appl. Phys.* **2018**, *51*, 145303.
[72] Z. Bo, K. Yu, G. Lu, P. Wang, S. Mao, J. Chen, *Carbon* **2011**, *49*, 1849.
[73] W. Takeuchi, H. Sasaki, S. Kato, S. Takashima, M. Hiramatsu, M. Hori, *J. Appl. Phys.* **2009**, *105*, 113305.
[74] A. N. Obraztsov, A. A. Zolotukhin, A. O. Ustinov, A. P. Volkov, Y. Svirko, K. Jefimovs, *Diamond Relat. Mater.* **2003**, *12*, 917.
[75] Y. Qi, B. Deng, X. Guo, S. Chen, J. Gao, T. Li, Z. Dou, H. Ci, J. Sun, Z. Chen, R. Wang, L. Cui, X. Chen, K. Chen, H. Wang, S. Wang, P. Gao, M. H. Rummeli, H. Peng, Y. Zhang, Z. Liu, *Adv. Mater.* **2018**, *30*, 1704839.
[76] N. Wei, Q. Li, S. Cong, H. Ci, Y. Song, Q. Yang, C. Lu, C. Li, G. Zou, J. Sun, Y. Zhang, Z. Liu, *J. Mater. Chem. A* **2019**, *7*, 4813.
[77] Y. Zhang, S. Deng, G. Pan, H. Zhang, B. Liu, X. L. Wang, X. Zheng, Q. Liu, X. Wang, X. Xia, J. Tu, *Small Methods* **2020**, *4*, 1900828.
[78] S. Shen, W. Guo, D. Xie, Y. Wang, S. Deng, Y. Zhong, X. Wang, X. Xia, J. Tu, *J. Mater. Chem. A* **2018**, *6*, 20195.
[79] X. Xia, S. Deng, D. Xie, Y. Wang, S. Feng, J. Wu, J. Tu, *J. Mater. Chem. A* **2018**, *6*, 15546.
[80] D. Xie, X. Xia, Y. Zhong, Y. Wang, D. Wang, X. Wang, J. Tu, *Adv. Energy Mater.* **2017**, *7*, 1601804.
[81] Z. Y. Zhang, W. Y. Li, M. F. Yuen, T. W. Ng, Y. B. Tang, C. S. Lee, X. F. Chen, W. J. Zhang, *Nano Energy* **2015**, *18*, 196.
[82] Y. Liu, X. Dong, P. Chen, *Chem. Soc. Rev.* **2012**, *41*, 2283.
[83] Z. Bo, K. Yu, G. Lu, S. Cui, S. Mao, J. Chen, *Energy Environ. Sci.* **2011**, *4*, 2525.
[84] L. Jiang, T. Yang, F. Liu, J. Dong, Z. Yao, C. Shen, S. Deng, N. Xu, Y. Liu, H. J. Gao, *Adv. Mater.* **2013**, *25*, 250.
[85] R. Prasher, *Proc. IEEE* **2006**, *94*, 1571.
[86] H. M. Fang, S. L. Bai, C. P. Wong, *Compos. Part A: Appl. Sci. Manufac.* **2018**, *112*, 216.
[87] Y. Fu, J. Hansson, Y. Liu, S. Chen, A. Zehri, M. K. Samani, N. Wang, Y. Ni, Y. Zhang, Z. B. Zhang, Q. Wang, M. Li, H. Lu, M. Sledzinska, C. M. S. Torres, S. Volz, A. A. Balandin, X. Xu, J. Liu, *2D Mater.* **2019**, *7*, 012001.
[88] B. C. Avram, K. Matin, S. Narumanchi, *J. Electron. Packag.* **2015**, *137*, 040803.
[89] R. Zhang, J. Cai, Q. Wang, J. Li, Y. Hu, H. Du, L. Li, *J. Electron. Packag.* **2014**, *136*, 011012.
[90] I. Dutta, R. Raj, P. Kumar, T. Chen, C. M. Nagaraj, J. Liu, M. Renavikar, V. Wakharkar, *J. Electron. Mater.* **2009**, *38*, 2735.
[91] S. H. Jeong, S. Chen, J. Huo, E. K. Gamstedt, J. Liu, S. L. Zhang, Z. B. Zhang, K. Hjort, Z. Wu, *Sci. Rep.* **2015**, *5*, 18257.
[92] K. Pashayi, H. R. Fard, F. Lai, S. Iruvanti, J. Plawsky, T. Borca Tasciuc, *Nanoscale* **2014**, *6*, 4292.
[93] H. Yu, L. Li, T. Kido, G. Xi, G. Xu, F. Guo, *J. Appl. Polym. Sci.* **2012**, *124*, 669.
[94] C. Yegin, N. Nagabandi, X. Feng, C. King, M. Catalano, J. K. Oh, A. J. Talib, E. A. Scholar, S. V. Verkhoturov, T. Cagin, A. V. Sokolov, M. J. Kim, K. Matin, S. Narumanchi, M. Akbulut, *ACS Appl. Mater. Interfaces* **2017**, *9*, 10120.
[95] B. Shen, W. Zhai, W. Zheng, *Adv. Funct. Mater.* **2014**, *24*, 4542.
[96] G. Xin, H. Sun, T. Hu, H. R. Fard, X. Sun, N. Koratkar, T. T. Borca, J. Lian, *Adv. Mater.* **2014**, *26*, 4521.
[97] Q. Wei, S. Pei, X. Qian, H. Liu, Z. Liu, W. Zhang, T. Zhou, Z. Zhang, X. Zhang, H. M. Cheng, W. Ren, *Adv. Mater.* **2020**, *32*, e1907411.
[98] L. Peng, Z. Xu, Z. Liu, Y. Guo, P. Li, C. Gao, *Adv. Mater.* **2017**, *29*, 1700589.
[99] N. Wang, M. K. Samani, H. Li, L. Dong, Z. Zhang, P. Su, S. Chen, J. Chen, S. Huang, G. Yuan, X. Xu, B. Li, K. Leifer, L. Ye, J. Liu, *Small* **2018**, *14*, 1801346.
[100] J. Xiang, L. T. Drzal, *Carbon* **2011**, *49*, 773.
[101] Q. Z. Liang, X. X. Yao, W. Wang, Y. Liu, C. P. Wong, *ACS Nano* **2011**, *5*, 2392.
[102] G. Li, X. Tian, X. Xu, C. Zhou, J. Wu, Q. Li, L. Zhang, F. Yang, Y. Li, *Compos. Sci. Technol.* **2017**, *138*, 179.
[103] J. D. Renteria, S. Ramirez, H. Malekpour, B. Alonso, A. Centeno, A. Zurutuza, A. I. Cocemasov, D. L. Nika, A. A. Balandin, *Adv. Funct. Mater.* **2015**, *25*, 4664.
[104] A. A. Balandin, *ACS Nano* **2020**, *14*, 5170.
[105] F. Yavari, H. R. Fard, K. Pashayi, M. A. Rafiee, A. Zamiri, Z. Yu, R. Ozisik, B. T. Theodorian, N. Koratkar, *J. Phys. Chem. C* **2011**, *115*, 8753.
[106] H. Fang, Y. Zhao, Y. Zhang, Y. Ren, S. L. Bai, *ACS Appl. Mater. Interfaces* **2017**, *9*, 26447.
[107] Q. Li, Y. Guo, W. Li, S. Qiu, C. Zhu, X. Wei, M. Chen, C. Liu, S. Liao, Y. Gong, A. K. Mishra, L. Liu, *Chem. Mater.* **2014**, *26*, 4459.
[108] G. Q. Xin, H. T. Sun, S. M. Scott, T. Yao, F. Y. Lu, D. Shao, T. Hu, G. K. Wang, G. Ran, J. Lian, *ACS Appl. Mater. Interfaces* **2014**, *6*, 15262.
[109] M. Zhou, T. Lin, F. Huang, Y. Zhong, Z. Wang, Y. Tang, H. Bi, D. Wan, J. Lin, *Adv. Funct. Mater.* **2013**, *23*, 2263.
[110] K. Wu, C. Lei, R. Huang, W. Yang, S. Chai, C. Geng, F. Chen, Q. Fu, *ACS Appl. Mater. Interfaces* **2017**, *9*, 7637.
[111] V. Goyal, A. A. Balandin, *Appl. Phys. Lett.* **2012**, *100*, 073113.
[112] G. Q. Qi, J. Yang, R. Y. Bao, Z. Y. Liu, W. Yang, B. H. Xie, M. B. Yang, *Carbon* **2015**, *88*, 196.
[113] J. Yang, X. Li, S. Han, Y. Zhang, P. Min, N. Koratkar, Z. Z. Yu, *J. Mater. Chem. A* **2016**, *4*, 18067.
[114] H. Jung, S. Yu, N. S. Bae, S. M. Cho, R. H. Kim, S. H. Cho, I. Hwang, B. Jeong, J. S. Ryu, J. Hwang, S. M. Hong, C. M. Koo, C. Park, *ACS Appl. Mater. Interfaces* **2015**, *7*, 15256.
[115] Z. Bo, H. R. Zhu, C.H. Ying, H.C. Yang, S. H. Wu, J. Kong, S. L. Yang, X. Wei, J. H. Yan, K. F. Cen, *Nanoscale* **2019**, *11*, 21249.

© 2020 Wiley-VCH GmbH

Shichen Xu received his B.S. degree from Northwest University in 2017. He is currently pursuing a Ph.D. degree at the College of Chemistry and Molecular Engineering, Peking University, in Beijing, China, under the guidance of Professor Jin Zhang. His current research interest mainly focuses on controllable growth of high-quality vertical graphene and its applications in thermal interface materials.

Jin Zhang received his Ph.D. from Lanzhou University in 1997. After a 2-year postdoctoral fellowship at the University of Leeds, UK, he returned to Peking University, where he was appointed associate professor (2000) and promoted to full professor in 2006. In 2013, he was appointed as Changjiang professor. His research focuses on the controlled synthesis and spectroscopic characterization of carbon nanomaterials.

© 2020 Wiley-VCH GmbH